Article

Developmental Cell

Antagonistic Self-Organizing Patterning Systems Control Maintenance and Regeneration of the Anteroposterior Axis in Planarians

Graphical Abstract

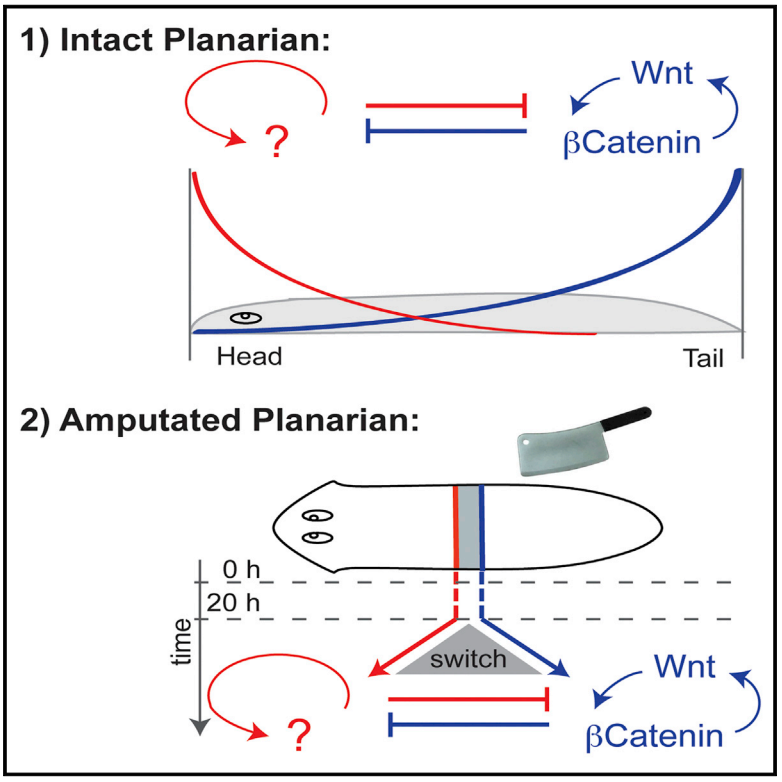

Authors

Tom Stückemann,
James Patrick Cleland,
Steffen Werner, ..., Benjamin Friedrich,
Frank Jülicher, Jochen Christian Rink

Correspondence

rink@mpi-cbg.de

In Brief

The regenerative abilities of planarians depend on long-range signaling gradients. Stückemann, Cleland, Werner et al. show that a tail-to-head Wnt gradient patterns the expression of genes, including gradient-forming Wnt pathway components. Mutual antagonism between the autoregulatory tail gradient and a self-organizing head patterning system governs global A/P patterning and pattern regeneration.

Highlights

- A tail-to-head Wnt signaling gradient exists along the planarian A/P axis
- The gradient patterns the expression of tail genes, including Wnt components
- Autoregulatory feedback governs gradient formation and maintenance
- The global A/P pattern depends on mutual tail-head antagonism

Stückemann et al., 2017, Developmental Cell *40*, 248–263
February 6, 2017
http://dx.doi.org/10.1016/j.devcel.2016.12.024

CellPress

CellPress

Developmental Cell
Article

Antagonistic Self-Organizing Patterning Systems Control Maintenance and Regeneration of the Anteroposterior Axis in Planarians

Tom Stückemann,[1,4] James Patrick Cleland,[1,4] Steffen Werner,[2,3,4] Hanh Thi-Kim Vu,[1] Robert Bayersdorf,[1] Shang-Yun Liu,[1] Benjamin Friedrich,[2,3] Frank Jülicher,[2] and Jochen Christian Rink[1,5,*]
[1]Max Planck Institute of Molecular Cell Biology and Genetics, Pfotenhauerstrasse 108, 01307 Dresden, Germany
[2]Max Planck Institute for the Physics of Complex Systems, Nöthnitzer Straße 38, 01187 Dresden, Germany
[3]Center for Advancing Electronics Dresden, Technische Universität Dresden, 01062 Dresden, Germany
[4]Co-first author
[5]Lead Contact
*Correspondence: rink@mpi-cbg.de
http://dx.doi.org/10.1016/j.devcel.2016.12.024

SUMMARY

Planarian flatworms maintain their body plan in the face of constant internal turnover and can regenerate from arbitrary tissue fragments. Both phenomena require self-maintaining and self-organizing patterning mechanisms, the molecular mechanisms of which remain poorly understood. We show that a morphogenic gradient of canonical Wnt signaling patterns gene expression along the planarian anteroposterior (A/P) axis. Our results demonstrate that gradient formation likely occurs autonomously in the tail and that an autoregulatory module of Wnt-mediated Wnt expression both shapes the gradient at steady state and governs its re-establishment during regeneration. Functional antagonism between the tail Wnt gradient and an unknown head patterning system further determines the spatial proportions of the planarian A/P axis and mediates mutually exclusive molecular fate choices during regeneration. Overall, our results suggest that the planarian A/P axis is patterned by self-organizing patterning systems deployed from either end that are functionally coupled by mutual antagonism.

INTRODUCTION

Animal body plans arise from the intricate interplay between cell-cell signaling and cell differentiation. Signaling events in the expanding embryonic cell mass initiate spatial patterns of cell differentiation, which commonly result in the generation of new signal sources (De Robertis, 2009; Meinhardt, 1996). Thus, the end of one patterning process initiates the next and the adult body plan emerges from a long hierarchy of patterns within patterns. However, development is not the only process capable of generating complex 3D assemblies of cells. Many adult animals have the ability to regenerate body parts lost to injury (Brockes and Kumar, 2008; Gemberling et al., 2013; Nacu and Tanaka, 2011) and planarian flatworms can even regenerate their entire body, including the brain and all other internal organs (Reddien and Sánchez Alvarado, 2004; Rink, 2013; Saló and Agata, 2012). In sharp contrast to development, regeneration does not have an invariant starting point, but ensues from randomly inflicted wounds. Regeneration therefore cannot proceed along a linear trajectory of patterns within patterns. Rather, it necessitates patterning systems capable of regenerating precisely the part of the pattern that is missing.

The robust and rapid regeneration of planarians exemplifies the challenges of regenerative patterning. If a worm is cut in half, the anterior piece regenerates a tail while the posterior piece regenerates a head. Yet, in response to a lateral incision, the animal simply heals the wound without regeneration. Consequently, regeneration requires cues that specify either head or tail regeneration, but only if these structures are actually missing. The abundant pluripotent stem cells of planarians (called neoblasts) drive new tissue formation during regeneration, but also the continuous turnover of all planarian cell types in non-regenerating animals (referred to as "intact" throughout this article) (Rink, 2013). Therefore, the maintenance of the planarian body plan also depends on the permanent presence of patterning signals to instruct location-specific stem cell progeny fate choices (e.g., eye differentiation only in the head). Overall, planarians provide a unique model system for studying patterning mechanisms, in terms of both the dynamic maintenance of an existing pattern and pattern regeneration in random tissue pieces.

Much recent planarian research has focused on identifying the patterning signals that define the planarian body plan and govern its regeneration. The highly conserved Wnt/β-catenin signaling pathway specifies the anteroposterior (A/P) head/tail axis. Wnt pathway inhibition by RNAi forces regeneration of heads irrespective of wound polarity (Gurley et al., 2008; Iglesias et al., 2008; Petersen and Reddien, 2008), whereas pathway activation is necessary and sufficient for tail regeneration (Gurley et al., 2008). In intact animals, gene expression patterns suggest high pathway activity in the tail and low activity in the head (Gaviño and Reddien, 2011; Gurley et al., 2008, 2010; Molina et al., 2007; Petersen and Reddien, 2009, 2011; Reddien et al., 2007; Reuter et al., 2015), multiple *β-catenin-1*(*RNAi*)- or *APC*(*RNAi*)-sensitive genes are expressed in tail-to-head gradients (Reuter et al., 2015), and a recent study indicates the existence of a tail-to-head β-catenin-1 protein gradient (Sureda-Gómez et al.,

2016). These data suggest that Wnt/β-catenin signaling not only specifies blastema fate during regeneration but that a Wnt signaling gradient may also pattern the A/P axis of intact animals (Adell et al., 2010; Meinhardt, 2009; Reuter et al., 2015). However, whether the gradient "patterns" gene expression and how it obtains its shape remain open questions. Furthermore, it is unclear whether fundamentally one mechanism patterns the entire A/P axis (e.g., a global Wnt gradient specifying "head" at low and "tail" at high signal levels) or whether molecularly distinct mechanisms pattern specific regions of the A/P axis (e.g., head, trunk, tail). A mechanistic view of planarian A/P patterning is therefore still lacking.

Toward this goal, we here developed tools to quantify Wnt signaling and A/P gene expression patterns in planarians. We find that Wnt signaling establishes a global tail-to-head gradient and that the Wnt gradient patterns gene expression along the A/P axis. The Wnt gradient in the tail can exist independently of the head, and both gradient maintenance and regeneration involve extensive autoregulatory feedback in the form of Wnt-mediated Wnt expression. Furthermore, the Wnt gradient in the tail limits the size of gene expression domains in the head and regulatory antagonism between head and tail also governs pattern regeneration. Overall, our results suggest a model in which maintenance and regeneration of the planarian A/P pattern involve mutual antagonism between the self-organizing Wnt gradient in the tail and a similarly self-organizing patterning system in the head.

RESULTS

A Wnt Signaling Gradient along the Planarian A/P Axis

Canonical Wnt signaling generally involves the stabilization of the intracellular transcription factor β-catenin in the presence of activating Wnt ligands. Planarians have segregated the conserved signaling and cell adhesion functions of β-catenin into separate genes (Smed-β-catenin-1 for signaling; Smed-β-catenin-2 for cell adhesion) (Chai et al., 2010). Therefore, β-catenin-1 protein abundance changes could provide a useful readout of planarian Wnt pathway activity, prompting us to generate monoclonal antibodies against Smed-β-catenin-1. The antibodies recognize a single band of approximately the predicted size, which decreased or increased under *β-catenin-1*(*RNAi*) or *APC*(*RNAi*), thus indicating specificity (Figure 1A). Since our antibodies did not work in immunofluorescence (data not shown), we instead developed a quantitative western blotting assay (see STAR Methods). Titration experiments with recombinant β-catenin-1 established a detection limit in the picogram range and linear detection up to 1.5 ng of β-catenin-1 per lane (Figure 1B), thus demonstrating both the sensitivity and utility of our Smed-β-catenin-1 (abbreviated as β-catenin or β-cat-1 from now on) quantification assay.

To identify putative Wnt signaling patterns along the planarian A/P axis, we sliced worms into ten slices and quantified the amount of β-catenin in each slice. Interestingly, we detected a smooth β-catenin abundance profile, with highest levels in the tail tip and lowest levels in the head (Figure 1C, blue trace). Both the profile shape and amplitude were highly reproducible, with a 4-fold abundance difference between head and tail tip and statistically significant differences between center and head tip (Figure 1C). Importantly, *β-catenin* transcript levels were uniform throughout most of the animal and even increased slightly in the head (Figure 1C, red trace). Therefore, these data demonstrate the existence of a post-transcriptional tail-to-head gradient of β-catenin along the planarian A/P axis.

If the β-catenin gradient were to reflect Wnt pathway activity, then its shape should depend on the distribution of pathway components. Multiple planarian Wnt ligands and the conserved Wnt sorting receptor *evi/wntless* (referred to as *evi* from now on) (Bartscherer et al., 2006; Bänziger et al., 2006) are known to be expressed at the tail tip (Figure 1D) or in long tail-to-head expression gradients in the body wall musculature (Figures 1E–1I, left panels) (Adell et al., 2009; Witchley et al., 2013). The nine Smed-Frizzled (fzd) receptors display a similar range of expression patterns (Figures S1A–S1C and 1J). We used single-molecule transcript counting (Geiss et al., 2008) in serial tissue slices to obtain quantitative A/P expression profiles of the tail-expressed *wnt* genes, *evi* and *fzd-1/2/7* as the receptor with the strongest influence on tail β-catenin levels (Figures 1D–1J, S1D, and S1E). Interestingly, RNAi of each of these pathway activators strongly affected the β-catenin gradient, albeit with subtle differences in their effects (Figures 1D–1J, right panels). The strongest reduction was always observed in the tail, consistent with the Wnt expression profiles, yet effects in the head were also noticeable. Significantly, only *evi(RNAi)* reduced β-catenin levels as severely as *β-catenin*(*RNAi*). Quantitative degradation of β-catenin in the absence of secreted Wnt ligands directly demonstrates that the amount of β-catenin-1 indeed reports on planarian Wnt pathway activity. The β-catenin protein gradient along the A/P axis therefore reflects a gradient of Wnt signaling activity, which integrates the individual contributions of multiple Wnt ligands and receptors (Figures 1D–1J and S1F–S1H).

To obtain insights into the cell types in which these Wnt ligands elicit signaling, we quantified the β-catenin gradient after stem cell ablation by irradiation. Interestingly, measured β-catenin levels were already strongly reduced at 24 hr after irradiation (particularly in the tail) and decreased further until day 9 (Figure 1K). These results therefore indicate that the irradiation-sensitive and abundant planarian stem cells (~20%–30% of all planarian cells) (Baguñà and Romero, 1981) contribute a significant fraction of Wnt-stabilized β-catenin, which we could in fact directly demonstrate by western blotting of cell populations sorted by fluorescence-activated cell sorting (FACS) (Figure S2). Consistent with the Wnt responsiveness of neoblasts, we detected the expression of Wnt signal transduction machinery (e.g., *fzd-1/2/7*, *fzd-4-2*, *axin-1*) and also a Wnt ligand (*wnt11-4*) in a published dataset of FACS-purified cell types (Figure 1L). The generally uniform distribution of neoblasts along the planarian A/P axis and the broadly maintained stem cell marker expression under *wnt*(*RNAi*) (not shown) jointly demonstrates the existence of an organism-wide Wnt signaling gradient that is read out by stem cells and other cells.

Gene Expression Patterns along the A/P Axis

As a precondition for asking whether the Wnt signaling gradient patterns gene expression, we first thought to obtain a systematic overview of gene expression patterns along the planarian A/P axis. RNA sequencing (RNA-seq) on a series of 11 equidistantly spaced tissue slices (Figure 2A, top) yielded A/P expression

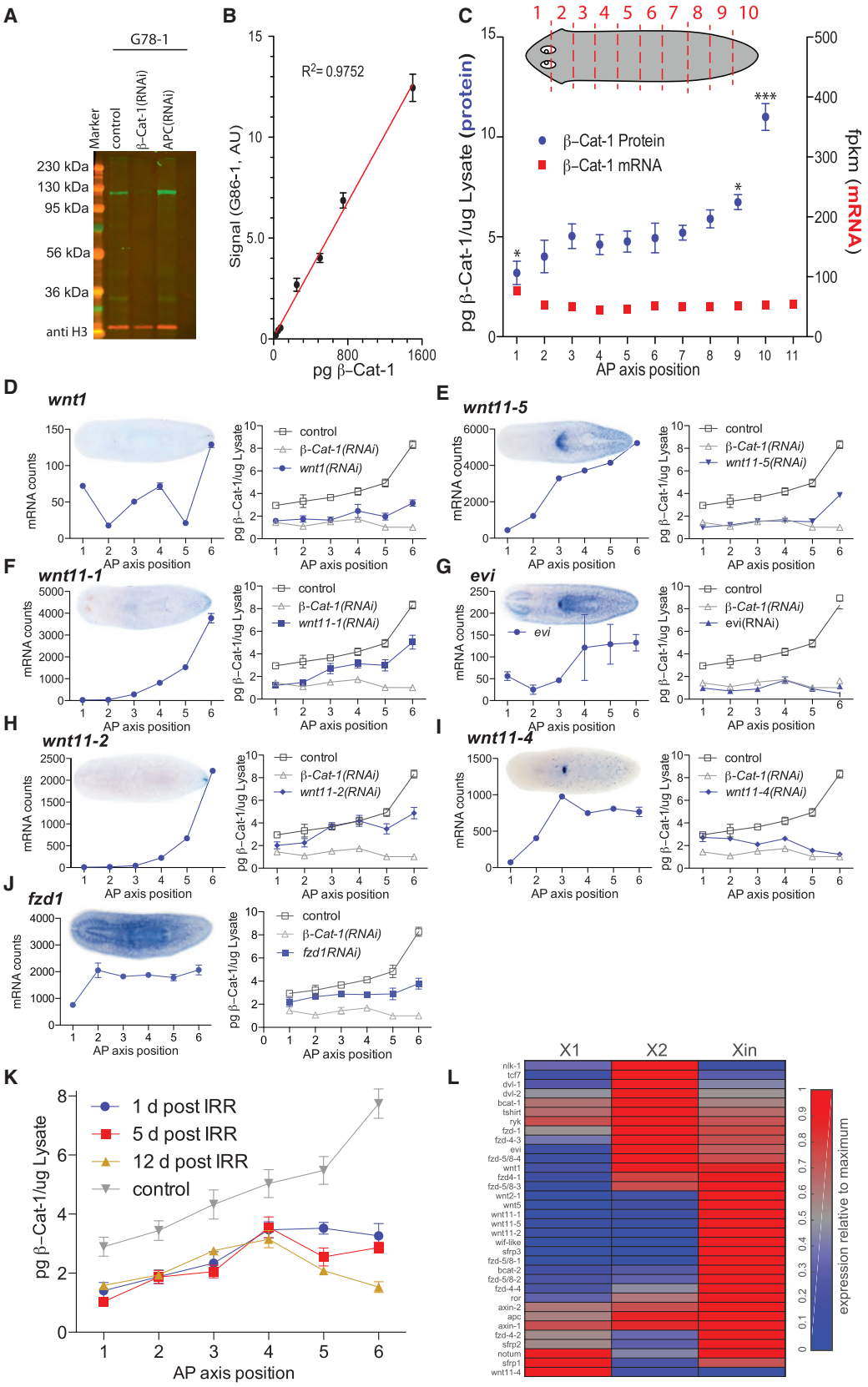

(legend on next page)

profiles for all planarian transcripts, which are available in PlanMine (Brandl et al., 2016). The application of an iterative clustering method to the pre-filtered expression profiles (see STAR Methods) yielded 14 well-defined gene expression clusters (Figures 2A and S3A; Table S1), the mean profiles of which (Figure 2B) represent the 14 most common gene expression domains along the planarian A/P axis. Collectively, these data reveal the broad zonation of the planarian A/P axis in head, trunk, and tail expression domains.

To link the expression profiles to planarian anatomy, we inspected the clusters for previously characterized genes (Figure 2A) and carried out whole-mount in situ hybridization on selected novel genes (Figures 2C and S3B). The spatial expression patterns were generally consistent with their mean cluster profiles; e.g., "neck genes" (cluster 2) were expressed in a narrow band of cells between brain and pharynx and the bell-shaped clusters 7 and 8 represent a population of putative secretory cells radially arranged around the pharynx (Figures 2B and 2C). Furthermore, our genome-wide survey confirmed long-range gene expression gradients as a common feature of planarian A/P patterning, including anterior-to-posterior "head gradient" genes (e.g., the *nou-darake* gene family) (Cebrià et al., 2002; Lander and Petersen, 2016; Scimone et al., 2016) or posterior-to-anterior "tail gradient" genes (e.g., the many muscle-expressed Wnt pathway components) (Gurley et al., 2010; Petersen and Reddien, 2009; Witchley et al., 2013). Interestingly, our RNA-seq data confirmed *wnt1* expression in the head (cluster 14), in addition to the tail-tip expression detectable by conventional in situ hybridization (Figure 2A; see also Figure 1D).

Toward our objective of analyzing patterning mechanisms, we added representative genes from the 14 clusters to our NanoString probe set. The resulting 99-gene array (Table S2) included muscle-expressed signaling pathway components ("PCG" genes) (Witchley et al., 2013), all Wnt pathway core components, stem cell markers, and multiple uncharacterized head/trunk/tail genes. Initial validation experiments on duplicate tail-tip samples confirmed the assay's sensitivity and reproducibility (e.g., detection of the "rare" Wnt1 transcript and an r^2 of 0.9996 between replicates; Figure S3C). Slicing planarians into six sections and subsequent NanoString quantification of the extracts provided A/P expression profiles of the panel genes (Figure 2D and Table S3) and thus a quantitative 1D representation of their corresponding whole-mount in situ patterns (Figure 2C). Jointly, our NanoString approach provided a quantitative overview of planarian A/P patterning and is thus an ideal experimental assay for investigating the mechanisms that establish the patterns.

The Wnt Gradient Patterns Gene Expression

To investigate the role of the Wnt signaling gradient in A/P patterning, we altered gradient shape (e.g., Figures 1D–1J) and quantified the resulting consequences on axial gene expression patterns (NanoString; Figure 2D). Specifically, we quantified β-catenin protein amounts and mRNA abundance of the 99 panel genes in each of six A/P slices under *wnt1*, *wnt11-1*, *wnt11-5*, *evi*, and *APC*(*RNAi*) (Figure 3A). The resulting 3,600 independent measurements (Table S3) provide a rich dataset for systematically analyzing the interplay between Wnt signaling activity and gene expression along the A/P axis.

We first asked which of the 99 genes correlated best with local β-catenin levels across all measurements (i.e., independent of A/P position). Figure 3B displays the genes ranked by their averaged correlation coefficients, ordered from lowest (anti-correlation) to highest (highly correlated). Eighteen genes were strongly correlated with β-catenin (>99% confidence), including many previously suspected Wnt signaling targets (Reuter et al., 2015). Many of the highly correlated genes were expressed in stem cells or stem cell progeny (e.g., *wnt11-4*, posterior Hox genes; Figure 1L), but others included known muscle-expressed genes (e.g., *fzd-4-1*, *wnt11-1*, *-2*) (Witchley et al., 2013). These results are therefore consistent with our previous identification of stem cells as major, but not exclusive, contributors to the measured Wnt signaling gradient (Figures 1K, 1L, and S2). To broadly correlate β-catenin sensitivity with planarian anatomy, we color coded the gene names in Figure 3B by head/trunk/tail cluster membership (Figure 2A) and analyzed the distribution of β-catenin correlation coefficients separately within each group (Figure 3C). Consistent with previous findings (Reuter et al., 2015), we found that Wnt signaling predominantly affected

Figure 1. β-Catenin Gradient along A/P Axis

(A) Fluorescence western blot probed with the anti-β-catenin-1 antibody G78-1 (green) and histone H3 (red). Molecular weight markers and RNAi conditions are as indicated.

(B) Titration of recombinant Smed-β-catenin-1 F1 by quantitative western blotting with mAb G78-1. Error bars denote SEM of two quantifications (two independent replicates, each in technical quadruplicates). The $R^2 = 0.9752$ of the linear regression fit (red) demonstrates linear detection between ~50 and 1,500 pg of β-catenin-1.

(C) Blue: β-catenin-1 abundance profile along the A/P axis, obtained by quantitative western blotting of ten serial A/P sections cut as cartooned and normalized by H3 (see Supplemental Information for details on quantification and normalization). Error bars denote SEM of three biological replicates, each determined as the mean of at least three technical replicates. Asterisks denote statistical significance of difference in β-catenin-1 levels between indicated A/P position and the center (position 5), at *95% or ***99% significance. Red: β-catenin-1 mRNA (FPKM [fragments per kilobase of transcript per million mapped reads], single replicate measurements) at indicated A/P positions by serial RNA-seq (Table S1).

(D–J) Expression patterns and β-catenin-1 gradient contributions of indicated Wnt pathway components. Left: whole-mount gene expression pattern and mRNA abundance profile (H3-normalized NanoString raw counts averaged between two biological replicates, now obtained from animals cut into six sections; error bars denote SEM). Right: β-catenin-1 gradient under knockdown of the indicated gene (blue trace), control (black trace), or *β-catenin-1*(*RNAi*) (gray trace). Error bars denote SEM of three biological replicates, each determined as the mean of at least three technical replicates.

(K) Irradiation sensitivity of Wnt signaling gradient. β-Catenin-1 gradient at indicated times post lethal irradiation, obtained by quantitative western blotting of six serial A/P sections cut as cartooned. Error bars denote SEM of three biological replicates, each determined as the mean of at least three technical replicates.

(L) Relative expression levels of Wnt pathway components in FACS sorted stem cell, progeny cell, and differentiated cell populations. The heatmap encodes fold difference relative to maximal expression, and hierarchical clustering was used for gene grouping. Based on raw data from Labbé et al. (2012).

See also Figures S1 and S2.

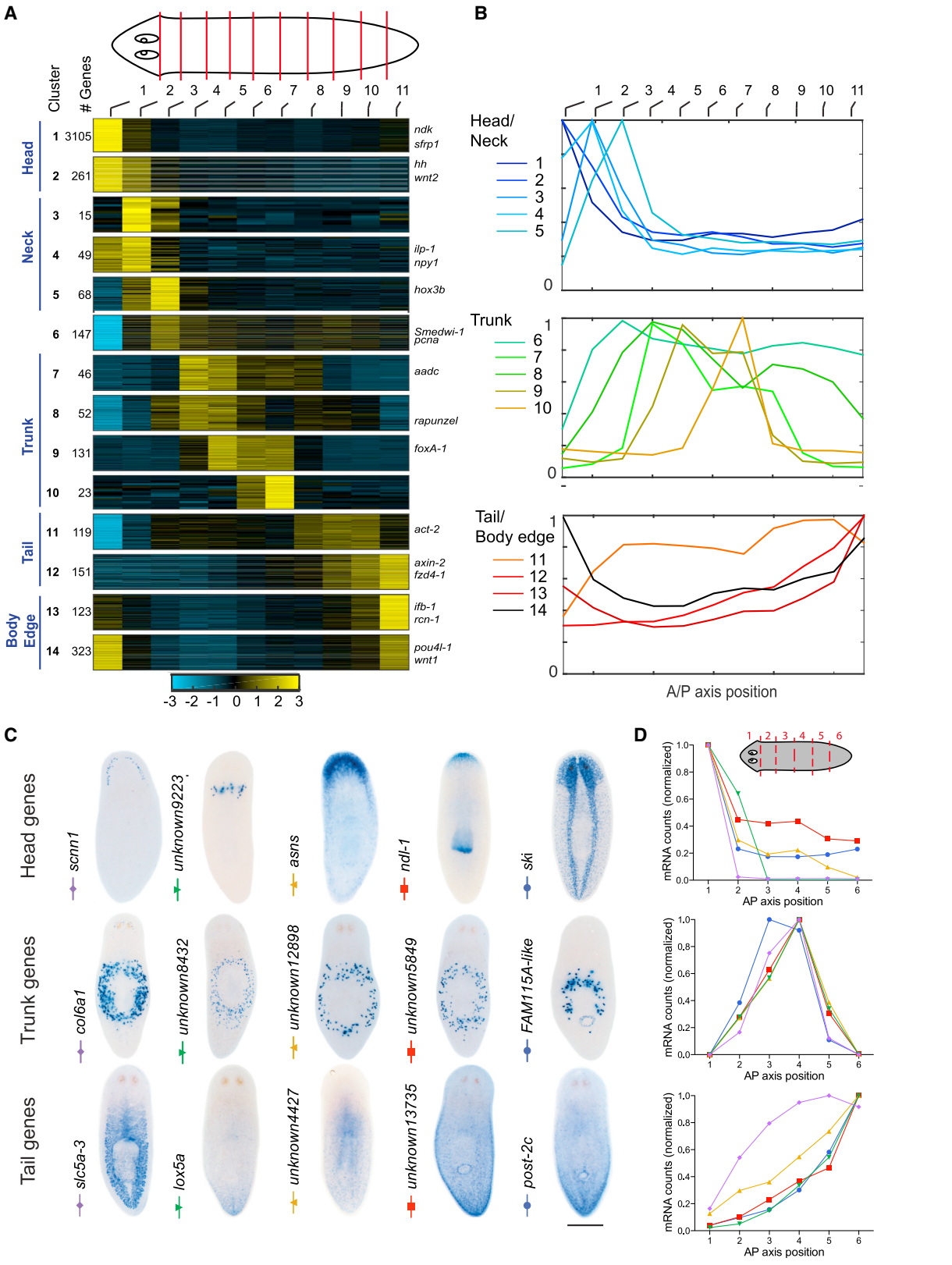

(legend on next page)

the expression of tail genes. However, not all tail genes in our dataset were Wnt sensitive (e.g., *ferritin*, *slc5a-3*, *unknown4427*, and *lactB*). Interestingly, the two most strongly anti-correlated genes (*unknown17916* and *ndk2*) were both head genes and head genes were generally enriched among anti-correlated genes (Figures 3B and 3C). Hence, these data suggest that Wnt signaling directly patterns the tail but also affects gene expression along the entire planarian A/P axis.

To investigate the extent to which the shape of the Wnt signaling gradient determines the shape of A/P gene expression profiles, we adapted our previously published principal component (PC) analysis (Werner et al., 2014) to the analysis of spatial gene expression profiles. Interestingly, we found that just two dominant expression profile modes (PC1 and PC2) were sufficient to accurately reconstruct the various profile shapes of the 71 genes in the dataset with >2× Min/Max variation along the A/P axis (Figure 3D). PC1 captures head/tail or tail/head gradient features (negative coefficient = head gradient; positive coefficient = tail gradient) and PC2 captures fluctuations in the trunk relative to the poles (negative coefficients = center gradient genes; positive coefficients = pole genes). Together, PC1 and PC2 accounted for 88% of the variation in the profiles. Plotting the relative contributions of PC1 and PC2 positioned the genes on a circular trajectory (Figure 3D), with the position encoding the shape of a gene's expression profile. To visualize the effect of β-catenin gradient changes on expression profiles, we connected the position of each gene under control and *wnt(RNAi)* by an arrow and further encoded expression level changes by arrow coloring. This analysis (Figure 3E) revealed three general trends. First, flattening of the Wnt gradient (flat-low: *evi*(*RNAi*); flat-high: *APC*(*RNAi*)) had the most severe effects on A/P gene expression patterns, with the long and centrally directed arrows suggesting corresponding flattening of expression profiles. Second, the expression pattern of trunk genes tended to shift posteriorly when Wnt signaling was inhibited (anti-clockwise rotation), but anteriorly when Wnt signaling was increased (*APC*(*RNAi*); clockwise rotation). Third, global antagonism was observed between head and tail genes, manifested in generally opposite arrow coloring between left (head genes) and right (tail genes) quadrants (particularly clear in *evi* and *APC*(*RNAi*)). Inspection of selected head, trunk, and tail expression profiles illustrated these points further. Head genes (Figure 3F) increased their average expression in the head up to 2-fold under Wnt inhibition, but also expanded posteriorly in some cases (Figures S4A and S4B). *APC(RNAi)* strongly decreased or even abolished head specificity of these profiles (Figure 3F). Many tail genes (Figure 3G), in contrast, became strongly upregulated and/or uniformly expressed along the A/P axis under *APC*(*RNAi*), but decreased average and individual expression levels under inhibited Wnt signaling. The trunk gene traces (Figure 3H) reflected the A/P shifts suggested by the shape mode analysis, which were further supported by similar likely position shifts of *unknown9923* (Figure S4C), a "neck" gene expressed between head and pharynx (Figure 2C).

Overall, our analysis demonstrated conclusively that the Wnt signaling gradient shapes axial gene expression. In addition, our data show that head/tail antagonism proportions the A/P axis, whereby weakening of the tail Wnt signaling increases the amplitude and range of head pattern genes while Wnt signaling increases expansion of tail patterns at the expense of the head pattern.

Wnt Gradient Autoregulation

Having demonstrated that the Wnt signaling gradient shapes gene expression along the planarian A/P axis, we next asked what shapes the Wnt signaling gradient. Several planarian Wnt inhibitors are prominently expressed in the head (Gurley et al., 2010; Petersen and Reddien, 2011), raising the possibility that head-mediated repression shapes the Wnt signaling gradient in the tail (Adell et al., 2010; Meinhardt, 2009). We therefore targeted two such Wnt inhibitors by RNAi and examined the effects on the shape of the Wnt signaling gradient. Both *notum*(*RNAi*) and *sFRP1*(*RNAi*) increased β-catenin levels in central regions (likely the pharynx) and *notum*(*RNAi*) additionally in the head, consistent with its known role in brain patterning (Hill and Petersen, 2015) (Figure 4A). However, neither knockdown resulted in the uniformly high Wnt signaling levels expected under a head repression mechanism. To conclusively rule out inhibitor redundancy or contributions of unknown genes, we asked whether a Wnt signaling gradient can exist in the complete absence of the head. We generated double-tailed animals using *ptc*(*RNAi*) (Figure 4B), which had only minor effects on Wnt gradient shape in intact animals (Figure S5A) (Rink et al., 2009). Double-tailed animals from regenerated *ptc*(*RNAi*) trunk pieces expressed the tail gradient gene and β-catenin target *fzd-4-1* at both ends and, importantly, still in a graded manner (Figure 4B). Direct measurement of the β-catenin gradient in double-tailed animals demonstrated that both tail tips initiated a gradient, with a low point in the center (Figure 4C), despite a lack of central Wnt inhibitor expression (Figure S5B). These data therefore conclusively rule out the head repression model, demonstrating instead that the tail Wnt gradient can form independently of the head.

Our previous demonstration that tail Wnt ligands shape the β-catenin gradient and that they themselves are expressed in gradients (except *wnt1*; Figures 1D–1J) suggested that the shape of the β-catenin gradient ultimately depends on the mechanisms that establish graded Wnt expression. Since we had already identified multiple Wnt pathway components among the β-catenin target genes (Figure 3B), we systematically analyzed pathway component expression across our entire

Figure 2. Gene Expression Patterns along the Planarian A/P Axis

(A) Clustered gene expression profiles obtained by RNA-seq of 11 serial A/P sections (single replicates), cut as cartooned. The heatmap encodes relative expression of the clustered profiles normalized by their SD. Left margin annotations: anatomical category, cluster number, and number of constituent genes. Right margin: known genes.

(B) Average maximum-normalized expression profiles of the 14 clusters, grouped and numbered as in (A).

(C) Whole-mount in situ hybridization expression patterns of selected head, trunk, and tail cluster members. Gene names as indicated. Scale bar, 0.5 mm.

(D) Maximum-normalized mRNA abundance profiles of the same genes as in (C), obtained by NanoString analysis of six serial A/P sections cut as cartooned (average of two replicates).

See also Figure S3.

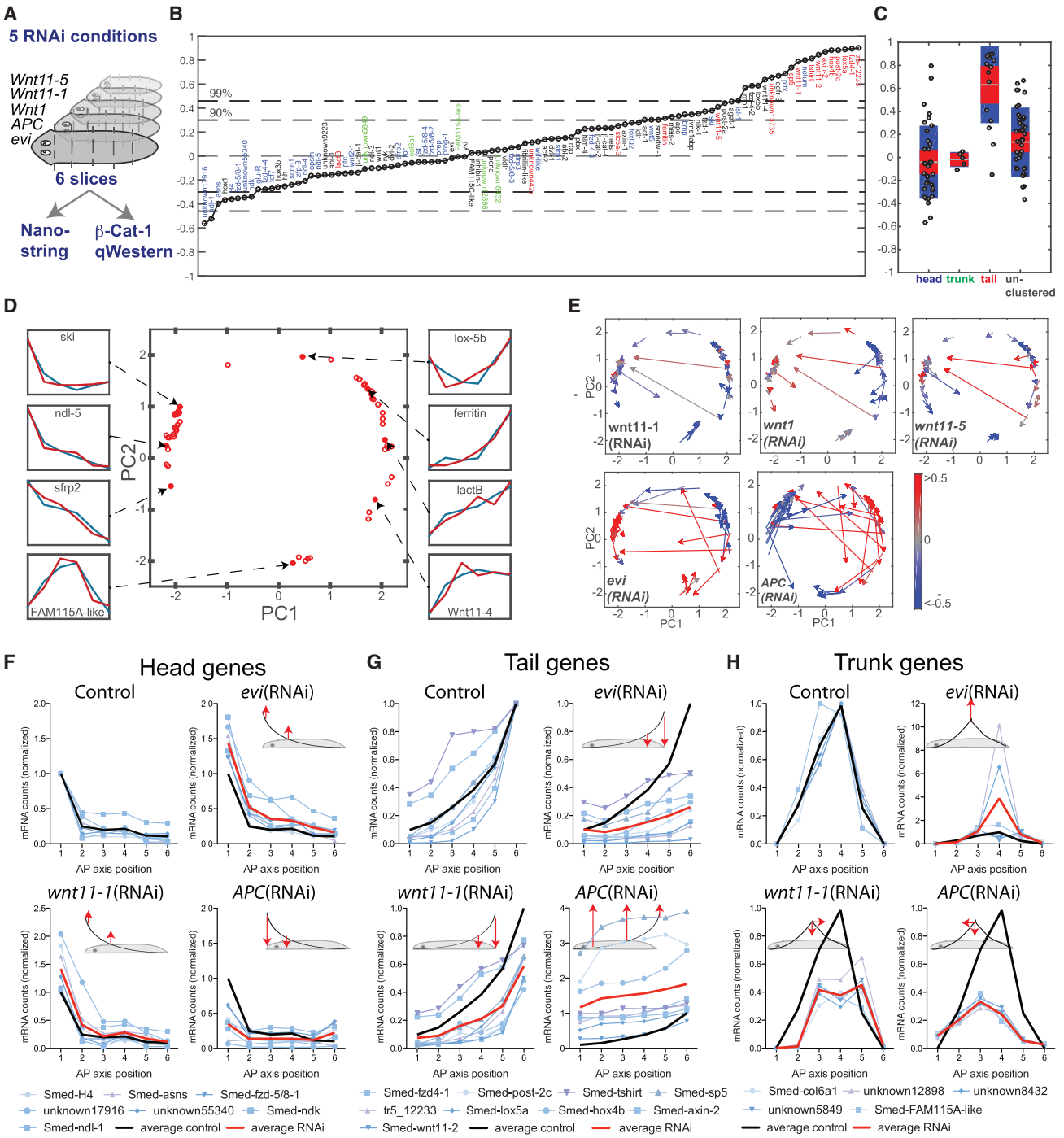

Figure 3. The Wnt Gradient Patterns Gene Expression along the Planarian A/P Axis

(A) Experimental design, involving six-slice quantification of β-catenin-1 amounts and mRNA counts of 99-gene NanoString panel under the indicated RNAi conditions (single replicates) and control (duplicates).

(B) Genes ranked by average correlation with β-catenin-1 levels in each slice. Gene-specific correlation coefficients were computed as correlation between the change in β-catenin-1 levels in a sample relative to the corresponding control sample and change in gene expression levels relative to the corresponding control sample, averaged across all RNAi conditions. Color coding: anatomical category (see Figure 2A). Blue, head genes clusters 1 and 2; green, trunk genes cluster 9; red, tail genes cluster 12.

(C) Box-plot analysis of correlation coefficients by A/P cluster category. Mean correlation coefficients for each group are indicated by a gray line, SEM (95% confidence interval) by red shading, and SD by blue shading.

(D) Quantitative analysis of gene expression profiles by principal component analysis (PCA). Red circles denote the PCA space position of the 58 genes in the dataset with >2-fold expression difference along their A/P profile and at least 50% of profile variance explained by the first two shape modes. Nanostring-measured (red) and PCA-reconstructed (blue) expression profiles of specific example genes in the plot are connected by arrows.

(legend continued on next page)

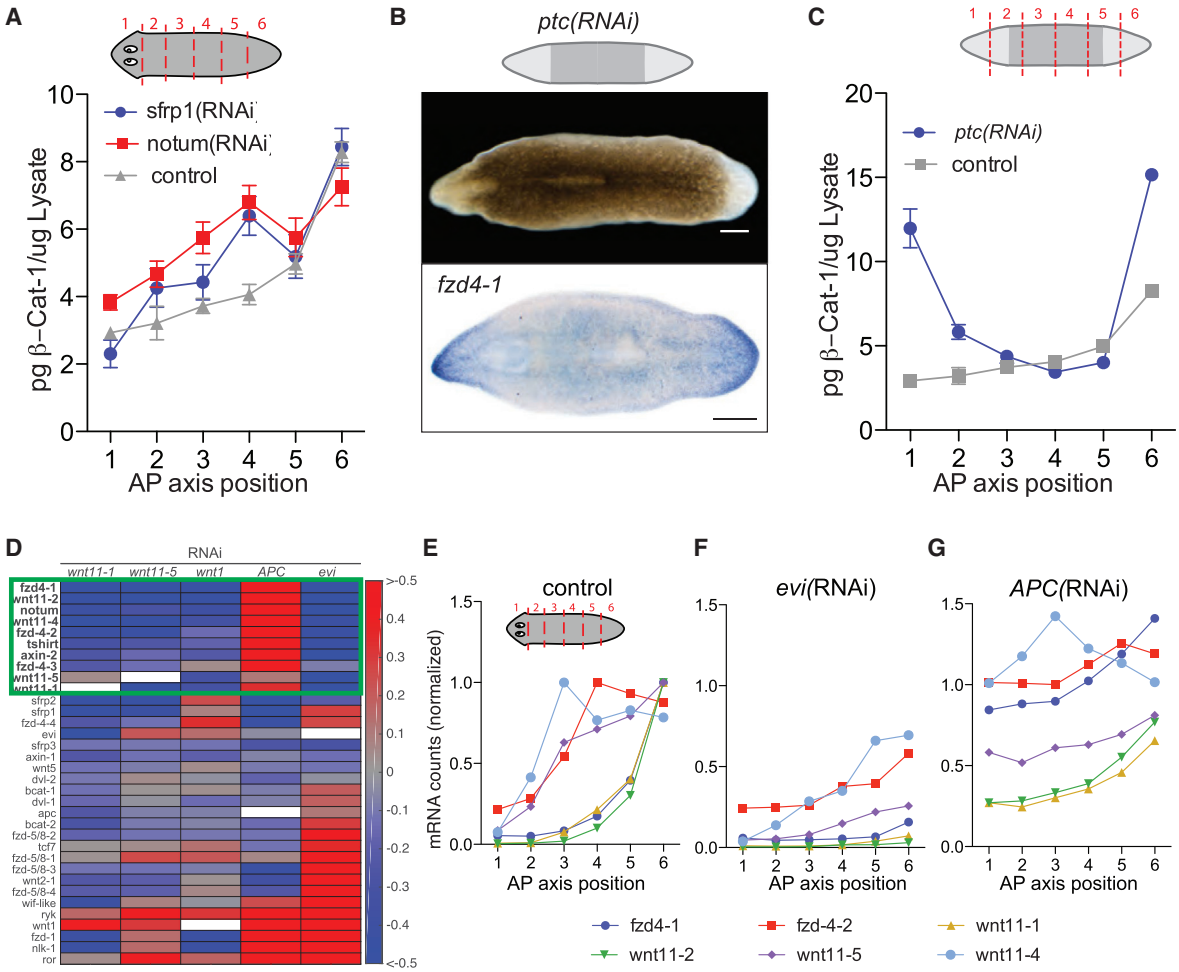

Figure 4. Wnt Gradient Autoregulation

(A) Effect of *notum*(*RNAi*) and *sFRP1*(*RNAi*) on β-catenin-1 gradient shape. Error bars denote SEM of three biological replicates, each determined as the mean of at least three technical replicates.

(B and C) Double-tailed regenerated trunk pieces from *ptc*(*RNAi*) animals. (B) Whole-mount in situ gene expression pattern of *fzd-4-1* expression 21 days post amputation. Scale bars indicate 500 μm. (C) β-Catenin-1 gradient quantification 14 days post amputation. Error bars denote SEM of two biological replicates, each determined as the mean of at least three technical replicates.

(D) Transcriptional Wnt pathway autoregulation in NanoString dataset from Figure 3A. The heatmap color scheme encodes the expression difference of Wnt pathway genes between control and indicated RNAi condition, averaged across all six A/P samples and normalized by mean expression level in control. Hierarchical clustering was used for gene grouping. Green box contains co-regulated tail gene module. White fields denote omitted measurements due to dsRNA contaminations of the respective mRNA measurements.

(E–G) NanoString A/P expression profiles of the indicated tail gene module members under the indicated RNAi conditions (control traces: average of two replicates; RNAi traces: single replicates). Profiles were normalized by the maximum of their corresponding control trace to reveal relative expression differences. See also Figure S5.

NanoString dataset. This analysis revealed a module of co-regulated Wnt pathway components that underwent collective down-regulation in response to all tested Wnt-inhibiting RNAi conditions, but upregulation under gain of function (*APC*(*RNAi*)) (Figure 4D). Intriguingly, all of the gradient-shaping tail Wnt ligands were part of this module, again with *wnt1* as the only

(E) PCA analysis of concerted gene expression profile changes under indicated RNAi conditions. Arrows indicate the PCA space shift (i.e., shape change) of gene profiles in response to RNAi; arrow color encodes the change in expression level relative to control (mean difference among six samples, normalized by mean control values).

(F–H) NanoString A/P expression profiles of indicated head (F), tail (G), and trunk (H) genes under the indicated RNAi conditions, normalized by their maximum count in control conditions (control traces: average of two replicates; RNAi traces: single replicates). The red line denotes the mean profile of each gene group under RNAi, and the black line the mean profile in control. Cartoons illustrate the relative deviation from control, with arrows indicating deviation direction. See also Figure S4.

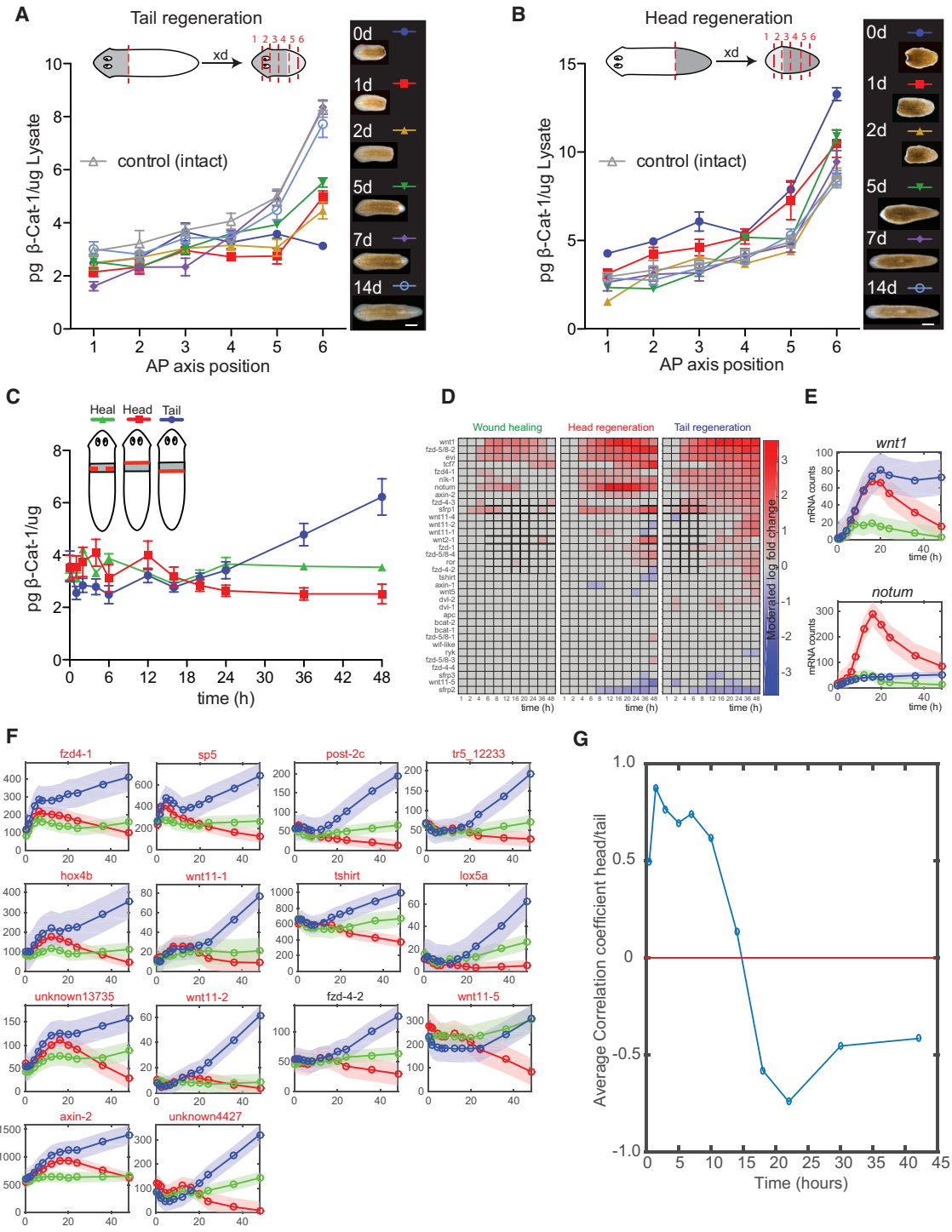

Figure 5. Wnt Gradient Regeneration

(A and B) β-Catenin-1 gradient regeneration time courses in head (A) and tail (B) fragments, cut as cartooned. Traces display the β-catenin-1 abundance profile along the regenerating fragments at the indicated days post amputation. Pictures show representative animals at the same time point. Error bars denote SEM of two biological replicates, each determined as the mean of at least three technical replicates. Scale bars, 0.5 mm.

(C) Wnt signaling dynamics in response to different wounds in the same anatomical area. Top: Cartoon illustrating location of the primary cut of the three wounding paradigms (red line); gray shading designates the tissue area excised for analysis of β-catenin-1 levels. Bottom: β-catenin-1 abundance at the indicated time points post primary cut and in the indicated wounding paradigms. Error bars denote SEM of two biological replicates, each determined as the mean of at least three technical replicates.

(legend continued on next page)

exception. In *evi*(*RNAi*) (Figures 4E and 4F), the muscle-expressed *wnt11-1*, *-2*, *-4*, and *fzd-4-1* were strongly downregulated, demonstrating Wnt-dependent Wnt expression. Consistently, the same genes were upregulated in *APC*(*RNAi*) along the entire A/P axis except for the extreme tail tip (Figure 4G), which coincides with the expression domain of the differentially regulated *wnt1*. Interestingly, the tail module also included the secreted Wnt inhibitor *notum*, which both our RNA-seq and NanoString datasets show to be expressed in the tail in a Wnt-dependent manner (Figure S5C). Conversely, *fzd-1/2/7* was strongly upregulated also under *evi*(*RNAi*), indicating non-exclusively Wnt-dependent regulation (Figure S5D). Overall, these data strongly indicate that the mechanism that establishes the graded expression of Wnt pathway activators is the Wnt gradient itself. Therefore, the Wnt signaling gradient likely shapes itself via an autoregulatory transcriptional module, involving positive and negative feedback loops (see Discussion).

Gradient Regeneration

To obtain further insights into the underlying mechanisms, we next analyzed the re-establishment of the Wnt gradient during regeneration. In head pieces regenerating a tail and thus a new gradient source (Figure 5A), wound site Wnt signaling was already significantly increased by 1 day post amputation (dpa), while more anterior regions still experienced signaling levels typical of the head. A second clear transition occurred between 5 and 7 dpa, when the signal intensity at the future tail tip approached its final level and gradient extension into pre-existing tissues became apparent. In tail pieces regenerating a head with the concomitant need to downregulate Wnt signaling (Figure 5B), β-catenin levels throughout the piece decreased during the first 24 hr and reached a low point between 2 and 5 dpa, reminiscent of *wnt11-5* expression kinetics in tail pieces (Gurley et al., 2010; Petersen and Reddien, 2009). In both head and tail pieces, gradient regeneration was completed by 14 dpa, together with the completion of morphological regeneration. The fact that the regenerated gradients were perfectly superimposable with pre-amputation controls despite the much smaller size of the regenerated animals was remarkable and indicates that the planarian A/P pattern may scale with body size.

Since Wnt signaling dynamics at tail- and head-regenerating wounds already differed at the earliest time point and since gradient re-establishment also appeared to initiate at the wound site (Figure 5A), we next carried out detailed time-course measurements of early wound site Wnt signaling dynamics. We compared head and tail regeneration-initiating cuts with lateral incisions in the same anatomical region (cartoon in Figure 5C) to distinguish between patterning-related and generally wound-induced signaling processes. Interestingly, none of the three wounding paradigms elicited clear and consistent Wnt signaling changes during the first 12 hr after wounding, with tissue contractions likely contributing to the early fluctuations (Figure 5C). From 24 hr onward, we detected a clear and tail regeneration-specific Wnt signaling increase (Figure 5C), consistent with the necessity and sufficiency of Wnt signaling for tail specification (Gurley et al., 2008). However, the initially largely parallel fluctuations of β-catenin-1 levels at head and tail wounds already started to diverge at 16 hr post amputation (hpa) (tail = up; head = down), indicating that the tail-specifying Wnt signal activation may already occur at ~16 hpa.

To address possible upstream causes and downstream consequences of this Wnt activation, we analyzed the gene expression dynamics of our 99-gene probe set under the exact same wounding paradigms and similar time points as in Figure 5C (Figure S6 and Table S4). We first focused on the expression dynamics of Wnt pathway components. Our data confirmed the early (<4 hr) wound-induced upregulation of *wnt1*, *sFRP1*, and *notum* (Figure 5D) (Gurley et al., 2010; Petersen and Reddien, 2009; Wurtzel et al., 2015) and identified *fzd-4-1*, *fzd-5/8-2*, *axin-2*, and *evi* as additional early-induced group members. These genes were generally induced more strongly at head/tail regenerating wounds compared with lateral incisions and displayed little head/tail specificity during the first 12 hr post wounding (e.g., *wnt1*; Figure 5E). The dramatic head-wound specificity of *notum* expression was also the only exception to this rule in our gene set (Wurtzel et al., 2015) (Figure 5E). In the face of such widespread and early induction of *wnt1* and other Wnt pathway components, it is interesting to note that we could not detect parallel changes in β-catenin levels, not even at tail wounds where *wnt1* expression should be unopposed by *notum* (Figure 5C). Whether this reflects a lack of Wnt1 translation at early time points or Wnt1 signaling activity that is not detectable by our assay constitute important questions regarding the triggering of tail regeneration (see Discussion).

Our analysis also revealed a second major change in gene expression beginning at ~16 hpa, comprising induction of a late and tail regeneration-specific group of Wnt pathway components (e.g., the tail module members *wnt11-1*, *-2*, and *-4*; Figure 5D), head/tail regeneration-dependent divergence of early group expression traces (e.g, *wnt1*; Figure 5E), and the sustained and tail regeneration-specific upregulation of all of the 18 highly correlated β-catenin target genes in our gene set (Figure 5F). Thus, consistent with the above β-catenin dynamics at head and tail wounds (Figure 5C), these data indicate that the tail-specifying Wnt signal is indeed activated at ~16 hpa. Further, the

(D) Wnt pathway component expression dynamics in RNA-seq datasets of the same experimental paradigms as cartooned in (C). The heatmap color scheme (right) encodes the moderated $\log_2$ fold change among three biological replicates relative to the zero time point. Hierarchical clustering was used to group genes with similar expression dynamics.

(E) Time course of *wnt1* and *notum* gene expression. Wounding paradigms and color coding are as shown in (C). The smoothed trend line represents the moving window average across the three replicates, and the shaded area 2 SDs about the smoothed trend.

(F) Gene expression time courses of tail genes, with color coding as in (C) and data representation as in (E).

(G) Cross-correlation over time between gene expression dynamics at head versus tail regenerating wounds. The 18 β-catenin target genes from Figure 3B ($p > 0.01$) were analyzed, and the blue line traces the correlation coefficient based on the relative expression change between successive measurements. Graph points therefore position between the time points measured in (D) to (F). The red line separates the plot into positive correlation values above (head and tail traces trend in the same direction) and anti-correlation below (head and tail traces of genes trend in opposite directions). y axis, normalized correlation coefficient; x axis, time (hr post amputation).

See also Figure S6.

concomitant rise of Wnt signaling activity and tail Wnt module expression (Figure 5F) suggests that the establishment of tail fate involves pathway autoactivation by Wnt-mediated Wnt expression.

Interestingly, at head-regenerating wounds β-catenin target genes were generally downregulated after 16 hpa (Figure 5F). To investigate this trend, we cross-correlated the head and tail regeneration traces of the 18 β-catenin target genes between successive time points. The resulting average tail/head cross-correlation curve (Figure 5G) quantitatively confirms the divergence of expression between the 12- and 16-hpa measurements (negative correlation coefficients = opposite gene regulation) and also largely wound type-independent gene regulation up to 12 hr (positive correlation coefficients = common gene regulation during the wound response). Inhibition of tail genes during head regeneration requires a head regeneration-specific mechanism that inhibits Wnt signaling and β-catenin target gene expression. Furthermore, the observed gene expression kinetics (up = tail, down = head) mirror exactly the switch-like role of Wnt signaling during regeneration (up, e.g., *APC*(*RNAi*) = tail; down, e.g., *β-catenin*(*RNAi*) = head) (Gurley et al., 2008). Our results therefore demonstrate that regeneration of the planarian A/P pattern involves a selection of mutually exclusive gene expression programs and suggests canonical Wnt signaling as the toggle mechanism. Our observations place the onset of pattern specification significantly earlier than previously thought (Wurtzel et al., 2015) and further highlight the importance of head/tail antagonism during pattern regeneration.

Planarian A/P Patterning at the Systems Level

Finally, we addressed the role of the Wnt signaling gradient from a systems perspective. Previous models of planarian A/P patterning have proposed an organism-wide Wnt gradient as sole patterning cue (Adell et al., 2010; Meinhardt, 2009; Umesono et al., 2013). Accordingly, Wnt signaling specifies both tail and head by activating the expression of tail genes and inhibiting the expression of head genes (Figure 6A). Globally high or low Wnt signaling levels should consequently lead to global expression of tail or head genes (Figure 6A). *APC*(*RNAi*) and *β-catenin*(*RNAi*) induce these states experimentally (Figure 6B), allowing us to explicitly test the single cue hypothesis.

We first examined the consequences of globally high Wnt signaling using a panel of posteriorly expressed marker genes as tail pattern readout (Figure S7A). *APC*(*RNAi*) worms displayed striking morphological alterations after 3 weeks of RNAi (Figure 6C), demonstrating the profound physiological consequences of Wnt gradient alterations. Interestingly, all tail marker genes were uniformly expressed throughout such animals (Figure 6C; see also Figure 3G). The loss of *slit1* expression along the midline and *wnt1* expression at the tip of the margin extensions further indicated a complete loss of all A/P pattern features, including head identity, exactly as predicted by the model (Figure 5A). To examine the consequences of globally low Wnt signaling, we used a panel of anterior marker genes as a head patterning readout (Figure S7B). As previously described, *β-catenin*(*RNAi*) induced supernumerary heads along the body margins (Gurley et al., 2008; Iglesias et al., 2008; Petersen and Reddien, 2008), which expressed our entire panel of head markers, including *notum* (Figure 6D). However, in sharp contrast to *APC*(*RNAi*), the head marker genes did not become uniformly expressed throughout the animal. First, marker expression remained confined to the head domains, except for *ndl-3*, which extends into the trunk region also in control animals (Figure S7B). Second, *slit1* expression was maintained, with each headlet nucleating its own midline. Third, within each headlet, the panel of head markers maintained approximate proximodistal expression patterns as in wild-type animals (Figures 6D and S7B). *Slit1* expression persisted even under the double-stranded RNA (dsRNA) injection protocol previously used to generate "radially hypercephalized" animals (Iglesias et al., 2008), demonstrating the maintenance of axial patterning even under the most severe downregulation of *β-catenin* (Figure S7C). Therefore, the planarian A/P pattern is not solely controlled by the Wnt gradient. Instead, the induction of multiple but well-patterned heads demonstrates that the head is patterned by β-catenin-independent mechanisms that are also capable of autonomous pattern initiation. Taken together, our results suggest that the planarian A/P patterning system involves at least two mechanistically distinct patterning systems deployed from either end of the A/P axis and functionally coupled via mutual inhibition (Figure 7).

DISCUSSION

Summary

Here, we investigate the mechanisms that pattern the planarian A/P axis and govern its regeneration. We find that both processes involve an autoregulatory Wnt signaling module capable of establishing a morphogenic gradient and of the autocatalytic re-establishment of tail identity during regeneration. Our data suggest functional antagonism between the Wnt gradient in the tail and an additional patterning system in the head as core mechanism of planarian A/P patterning.

A Morphogenic Wnt Gradient along the Planarian A/P Axis

Signaling gradients have long been discussed as a putative patterning mechanism of the planarian A/P axis (Adell et al., 2010; Morgan, 1905; Reuter et al., 2015; Witchley et al., 2013). We now demonstrate explicitly that a Wnt signaling gradient exists at the organismal scale and that this gradient patterns gene expression. We use the term "morphogenic gradient" to express the functional parallels with embryonic morphogen gradients, yet without necessarily implying parity in the underlying mechanisms. Our gradient quantification by western blotting averages Wnt signaling activity across all cell types. The A/P gradation of the Wnt signaling profile therefore demonstrates that planarian cells experience different Wnt signaling levels along the A/P axis, much like cells in early vertebrate embryos (Kiecker and Niehrs, 2001). Still, individual cell types may experience Wnt signaling levels different from the local average (e.g., in the brain) and individual Wnts may have specific cellular targets, consistent with recent reports of tail Wnt-specific RNAi phenotypes (Lander and Petersen, 2016; Scimone et al., 2016; Sureda-Gómez et al., 2015). However, our findings indicate that the abundant pluripotent planarian stem cells experience position-dependent levels of Wnt signaling and, consequently, position-specific expression of Wnt target genes. Consistent with a previous study (Reuter et al., 2015), we identified multiple planarian Hox genes as stem and progeny cell-expressed Wnt targets (Figure 3B). The highly

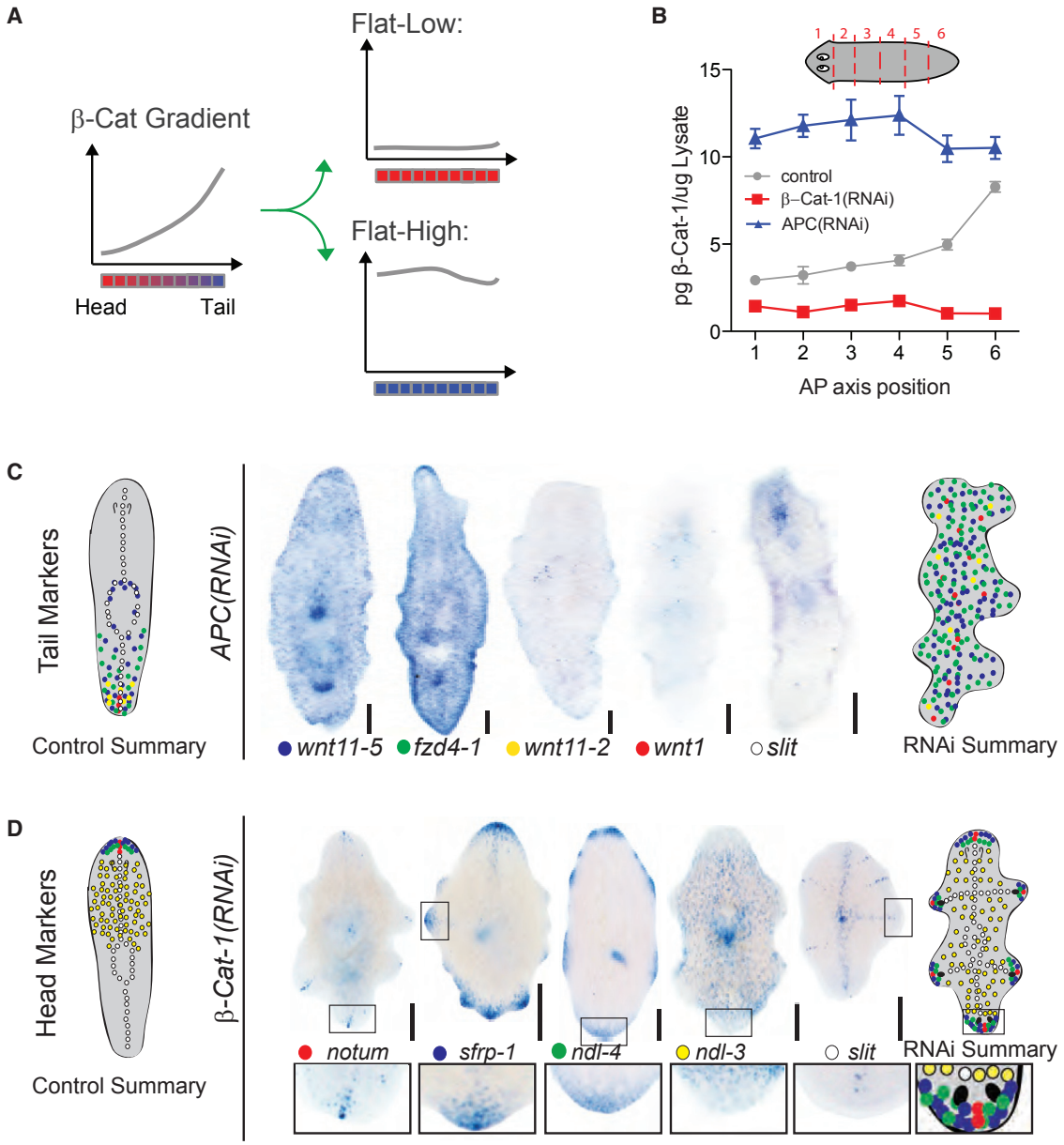

Figure 6. Systems Properties of Planarian A/P Patterning

(A) Left: schematic representation of Wnt gradient function as single A/P patterning cue. Right: predicted response upon globally high or low Wnt signaling.

(B) Globally high or low Wnt signaling achieved by *APC(RNAi)* or *β-catenin-1(RNAi)*. Error bars denote SEM of three biological replicates, each determined as the mean of at least three technical replicates.

(C) Whole-mount in situ hybridization of a tail + midline marker panel in *APC(RNAi)* animals treated as in (B). Gene names and symbols as indicated. Scale bar, 1 mm.

(D) Whole-mount in situ hybridization of a head + midline marker panel on APC(RNAi) animals treated as in (B). Gene names and symbols as indicated. Scale bar, 1 mm.

See also Figure S7.

conserved role of Hox genes in the regionalization of animal body plans (Mallo et al., 2010) suggests a likely mechanism for position-specific cell fate choices downstream of the Wnt gradient. The emerging view of a long-range Wnt signaling gradient converted into corresponding expression gradients of cell fate determinants in neoblasts provides a mechanistic framework for the maintenance of the planarian body plan in face of constant turnover. As such, our results also confirm key aspects of T.H. Morgan's hypothesis put forward in 1905, according to which "gradients of formative substances" provide the mechanistic basis of planarian body plan polarity (Morgan, 1905).

Self-Organizing Properties of the Wnt Gradient

In light of the morphogenic functions of the Wnt gradient, identifying the mechanisms that establish its shape become a key objective. Our results demonstrate that both gradient shape

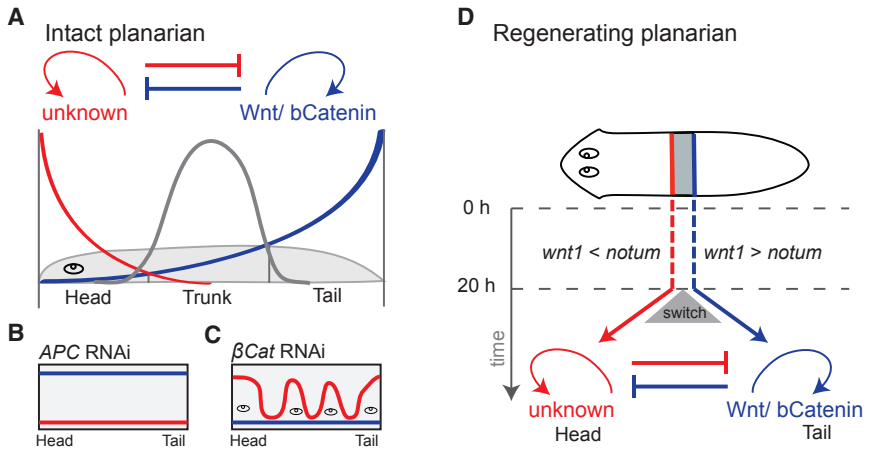

Figure 7. Model of Planarian A/P Patterning
Model of A/P patterning mechanisms in intact planarians (A), under Wnt gain and loss of functions (B and C), or during regeneration (D). See text for details.

and regeneration involve an autoregulatory tail Wnt module. The same module is also involved in gradient re-establishment during regeneration, and the maintenance of gradients in double-tailed animals demonstrates that gradient formation is likely an autonomous property of the tail. Furthermore, the "chicken and egg" relationship between A/P-graded Wnt expression shaping the gradient and the gradient shaping A/P-graded Wnt expression implies that the planarian Wnt signaling gradient literally shapes itself. Turing patterns provide a compelling mechanistic framework for self-organized gradient formation (Gierer and Meinhardt, 1972; Turing, 1952). Our observations of Wnt-dependent expression of *wnt11-1*, *-2*, *-4*, and *-5* (Figures 4D–4G), *wnt* expression in the form of gradients rather than narrow source regions (with the exception of *wnt1*, Figures 1D–1I), and likely Wnt-activated *wnt* re-expression during tail regeneration are all consistent with the expected properties of a self-activating activator in a Turing system. Further, our finding that the secreted Wnt inhibitor *notum* is expressed in the tail contrary to its seemingly head-specific in situ expression pattern (Petersen and Reddien, 2011) and that its expression is similarly Wnt dependent (Figure S5C) provides a candidate molecule for the crucial inhibitor function in a Turing system. It is therefore entirely plausible that the shape of the planarian Wnt gradient results from the self-organization of the tail Wnt module as a Turing pattern, with the *wnt*-expressing muscle layer (Witchley et al., 2013) as permissive platform for pattern formation.

A further attractive aspect of this hypothesis is that Turing patterns are intrinsically regenerative, since gradient source specification is a systems property that does not require external determinants (Gierer and Meinhardt, 1972; Werner et al., 2015). Our observation that tail gradient regeneration is initiated by a concomitant rise in Wnt signaling and *wnt* expression at ~16 hpa is compatible with self-activated source regeneration. Further, the temporal reproducibility of tail Wnt module activation (Figure 5C) indicates the existence of a trigger mechanism, of which *wnt1* and *notum* are likely components. *Wnt1* is necessary for tail specification and induced at all wounds long before 16 hpa (Figures 5D and 5E) (Adell et al., 2009; Petersen and Reddien, 2009). In contrast, the Wnt inhibitor *notum* is only induced at anterior-facing wounds, thus providing a plausible scenario for restricting the likely Wnt1-dependent initiation of tail regeneration to non-notum-expressing posterior-facing wounds (Petersen and Reddien, 2011). The pervasive expression of Wnt core pathway components (e.g., *fzd-1/2/7*, *disheveled*, *APC*, *β-catenin*; Table S1) is conceptually significant, as it enables the Wnt-1-dependent triggering of tail formation at wound sites anywhere in the animal. Significantly, *wnt1* is not a component of the autoregulatory tail Wnt module (Figure 4D) and may even be transcriptionally antagonized by β-catenin (Table S3). Therefore, it seems unlikely that the regeneration of the planarian Wnt gradient is the result of a solely self-contained Turing mechanism (i.e., entirely β-catenin regulated). Rather, we envisage the interplay between autoregulatory and systems-external (i.e., non-β-catenin dependent) mechanisms as basis of planarian pattern regeneration. Conceptually, such a system could provide additional safeguards against the inherent tendency of autoregulatory systems to amplify random fluctuations (Werner et al., 2016), the catastrophic consequences of which are graphically illustrated by the multi-headed *β-catenin(RNAi)* animals (Figure 6D).

Tail versus Head

Tail specification and patterning via the Wnt gradient raises the question of how the planarian head is specified and patterned. The necessity and sufficiency of increased or decreased Wnt signaling for tail or head regeneration (Gurley et al., 2008) establishes that head and tail are not only topological but also regulatory opposites. Accordingly, the molecular definition of "head" could simply amount to the absence of "tail" or, more specifically, to the anterior end of the β-catenin gradient. However, our results strongly suggest that large-scale head patterning is accomplished in a β-catenin-independent manner. Much like double-tailed animals can maintain the tail pattern in the absence of a head, double-headed planarians can maintain the head pattern in the absence of a tail (Gurley et al., 2008; Petersen and Reddien, 2008). The occurrence of ectopic but axially patterned heads under uniformly flat β-catenin levels (Figure 6C) further rules out head patterning as the inverse of the tail gradient profile. Rather, these observations suggest that the planarian head also constitutes a self-organized patterning system. Multiple signaling pathways have been implicated in planarian head specification or patterning, yet the mechanisms mediating spatial pattern formation remain unclear (Cebrià et al., 2002; Lander and Petersen, 2016; Nogi and Levin, 2005; Nogi et al., 2009; Scimone et al., 2016; Umesono et al., 2013). However, we show that the head and tail patterns are functionally coupled. Specifically, our data suggest a model of planarian A/P patterning in which mutual inhibition between head and tail signaling systems proportions the A/P axis and mediates

mutually exclusive blastema fate choices during regeneration (Figures 7A–7D).

Model

We show that a Wnt/β-catenin gradient (Figure 7, blue) patterns the tail, while a β-catenin-independent gradient-forming system (Figure 7, red) patterns the head. Head and tail signaling systems inhibit each other mutually, likely at the level of β-catenin (Figure 7, blunt arrows). Trunk genes (Figure 7, gray) are activated at the low point between both systems and additional pattern elements (e.g., "neck" genes or organs) may be positioned via similar combinatorial pattern use. Our model entails proportioning of the planarian A/P axis by mutual antagonism between head and tail patterns and consequent head pattern size changes upon interference with the posterior tail gradient (Figure 3). Further, it explains the global assumption of tail fate and complete A/P pattern loss under forced Wnt activation in *APC(RNAi)* (Figure 7B) and the appearance of supernumerary but axially patterned heads in *β-catenin(RNAi)* as the result of self-organized head pattern initiation in the now globally permissive tissue environment upon removal of the inhibitory tail Wnt signal (Figure 7C). During regeneration, the mutual antagonism between autoregulatory signaling systems governs pattern regeneration, this time in the form of activation of alternative and mutually exclusive gene expression programs, likely by Wnt1/notum-mediated triggering of a β-catenin-dependent gene module (Figure 7D). Our model also provides a mechanistic framework for the recent reports of coordination between head and tail gene expression gradients (Lander and Petersen, 2016; Scimone et al., 2016). Conversely, the reported effect of the trunk-expressed *ptk7* on trunk and tail patterning raises the interesting possibility that trunk signals may in turn actively influence head and tail patterns (Lander and Petersen, 2016).

Parallels between Planarian and Embryonic Patterning

By demonstrating that adult planarians make use of long-range signaling gradients to spatially coordinate gene expression, our findings establish interesting parallels to the morphogen gradients that pattern developing embryos. Patterning of the early *Drosophila* embryo by long-range gradients deployed from either pole and subsequent combinatorial intercalation of progressively more fine-grained pattern elements (Jaeger, 2011) is conceptually similar to planarian A/P patterning. However, planarians pose additional challenges not routinely encountered by embryos, including the permanent rather than transient maintenance of signaling gradients, pattern re-establishment in tissue pieces of arbitrary size and geometry, or the inherent need for pattern scaling due to their dramatic food supply-dependent variations in body size (Baguñà et al., 1990). Planarians therefore present an opportunity to study the molecular basis of pattern establishment and scaling in spatial dimensions beyond the effective range of diffusive signal propagation, both of which constitute important problems in understanding body plan morphogenesis.

STAR★METHODS

Detailed methods are provided in the online version of this paper and include the following:

- KEY RESOURCES TABLE
- CONTACT FOR REAGENT AND RESOURCE SHARING
- EXPERIMENTAL MODEL AND SUBJECT DETAILS
- METHOD DETAILS
  - Animals, Cloning, and RNAi
  - Recombinant Proteins and Antibody Production
  - RNA Extraction and RNA Sequencing
  - NanoString Gene Expression Analysis
  - Quantitative Western Blotting
  - In Situ Hybridization
  - Analysis of β-catenin in FACS-sorted Cells
  - Imaging
- QUANTIFICATION AND STATISTICAL ANALYSIS
  - RNAseq Analysis
  - A/P Gene Expression Profile Filtering
  - A/P Gene Expression Profile Clustering
  - Quantitative Western Blotting Analysis
- DATA AND SOFTWARE AVAILABILITY

SUPPLEMENTAL INFORMATION

Supplemental Information includes seven figures and six tables can be found with this article online at http://dx.doi.org/10.1016/j.devcel.2016.12.024.

AUTHOR CONTRIBUTIONS

Conceptualization: J.C.R., F.J., B.F.; Methodology: T.S., S.-Y.L.; Formal Analysis: S.W., T.S.; Investigation: T.S., J.P.C., H.T.-K.V., S.-Y.L., R.B.; Writing – Original Draft: J.C.R.; Writing – Review & Editing: J.C.R., S.W., J.P.C., F.J., B.F.; Visualization: J.C.R., T.S., S.W., H.T.-K.V.; Funding Acquisition: J.C.R., F.J.

ACKNOWLEDGMENTS

We thank Stephanie von Kannen for technical assistance and Heino Andreas for animal care; Iain Patten and Profs. Elisabeth Knust and Elly Tanaka for comments on the manuscript; and the late Hans Meinhardt for discussions. Further, we would like to thank the following Services and Facilities of the MPI-CBG for their support: Antibody, Light Microscopy, DNA Sequencing, Bioinformatics & Scientific Computing, Grants Office, DNA Microarray and the Deep Sequencing Group (SFB 655/BIOTEC) and Andreas Dahl for RNA sequencing. This work was supported by BMBF Grant FKZ 0316169, "Virtual Planarian."

Received: July 9, 2016
Revised: November 5, 2016
Accepted: December 30, 2016
Published: February 6, 2017

REFERENCES

Adell, T., Saló, E., Boutros, M., and Bartscherer, K. (2009). Smed-Evi/Wntless is required for beta-catenin-dependent and -independent processes during planarian regeneration. Development *136*, 905–910.

Adell, T., Cebrià, F., and Saló, E. (2010). Gradients in planarian regeneration and homeostasis. Cold Spring Harb. Perspect. Biol. *2*, a000505.

Baguñà, J. (1976). Mitosis in the intact and regenerating planarian Dugesia mediterranea n.sp. I. J. Exp. Zool. *195*, 53–64.

Baguñà, J., and Romero, R. (1981). Quantitative analysis of cell types during growth, degrowth and regeneration in the planarians *Dugesia mediterranea* and *Dugesia tigrina*. Hydrobiologia *84*, 184–191.

Baguñà, J., Romero, R., Saló, E., Collet, J., Auladell, C., Ribas, M., Riutort, M., Garcia-Fernandez, J., Burgaya, F., and Bueno, D. (1990). Growth, degrowth and regeneration as developmental phenomena in adult fresh water

planarians. In Experimental Embryology in Aquatic Plants and Animals, H.-J. Marthy, ed. (Plenum Press), pp. 129–162.

Bänziger, C., Soldini, D., Schütt, C., Zipperlen, P., Hausmann, G., and Basler, K. (2006). Wntless, a conserved membrane protein dedicated to the secretion of Wnt proteins from signaling cells. Cell *125*, 509–522.

Bartscherer, K., Pelte, N., Ingelfinger, D., and Boutros, M. (2006). Secretion of Wnt ligands requires Evi, a conserved transmembrane protein. Cell *125*, 523–533.

Brandl, H., Moon, H., Vila-Farré, M., Liu, S.-Y., Henry, I., and Rink, J.C. (2016). PlanMine — a mineable resource of planarian biology and biodiversity. Nucleic Acids Res. *44*, D764–D773.

Brockes, J.P., and Kumar, A. (2008). Comparative aspects of animal regeneration. Annu. Rev. Cell Dev. Biol. *24*, 525–549.

Cebrià, F., Kobayashi, C., Umesono, Y., Nakazawa, M., Mineta, K., Ikeo, K., Gojobori, T., Itoh, M., Taira, M., Sánchez Alvarado, A., et al. (2002). FGFR-related gene nou-darake restricts brain tissues to the head region of planarians. Nature *419*, 620–624.

Chai, G., Ma, C., Bao, K., Zheng, L., Wang, X., Sun, Z., Saló, E., Adell, T., and Wu, W. (2010). Complete functional segregation of planarian beta-catenin-1 and -2 in mediating Wnt signaling and cell adhesion. J. Biol. Chem. *285*, 24120–24130.

De Robertis, E.M. (2009). Spemann's organizer and the self-regulation of embryonic fields. Mech. Dev. *126*, 925–941.

Eisenhoffer, G.T., Kang, H., and Sánchez Alvarado, A. (2008). Molecular analysis of stem cells and their descendants during cell turnover and regeneration in the planarian *Schmidtea mediterranea*. Cell Stem Cell *3*, 327–339.

Ester, M., Kriegel, H.P., Sander, J., and Xu, X. (1996). A Density-Based Algorithm For Discovering Clusters in Large Databases with Noise. KDD Proceedings 1996 (AAAI). http://www.aaai.org/Papers/KDD/1996/KDD96-037.pdf.

Gaviño, M.A., and Reddien, P.W. (2011). A Bmp/Admp regulatory circuit controls maintenance and regeneration of dorsal-ventral polarity in planarians. Curr. Biol. *21*, 294–299.

Geiss, G.K., Bumgarner, R.E., Birditt, B., Dahl, T., Dowidar, N., Dunaway, D.L., Fell, H.P., Ferree, S., George, R.D., Grogan, T., et al. (2008). Direct multiplexed measurement of gene expression with color-coded probe pairs. Nat. Biotechnol. *26*, 317–325.

Gemberling, M., Bailey, T.J., Hyde, D.R., and Poss, K.D. (2013). The zebrafish as a model for complex tissue regeneration. Trends Genet. *29*, 611–620.

Gierer, A., and Meinhardt, H. (1972). A theory of biological pattern formation. Kybernetik *12*, 30–39.

Gurley, K.A., Rink, J.C., and Sánchez Alvarado, A. (2008). Beta-catenin defines head versus tail identity during planarian regeneration and homeostasis. Science *319*, 323–327.

Gurley, K.A., Elliott, S.A., Simakov, O., Schmidt, H.A., Holstein, T.W., and Sánchez Alvarado, A. (2010). Expression of secreted Wnt pathway components reveals unexpected complexity of the planarian amputation response. Dev. Biol. *347*, 24–39.

Hill, E.M., and Petersen, C.P. (2015). Wnt/Notum spatial feedback inhibition controls neoblast differentiation to regulate reversible growth of the planarian brain. Development *142*, 4217–4229.

Iglesias, M., Gómez-Skarmeta, J.L., Saló, E., and Adell, T. (2008). Silencing of Smed-betacatenin1 generates radial-like hypercephalized planarians. Development *135*, 1215–1221.

Jaeger, J. (2011). The gap gene network. Cell Mol. Life Sci. *68*, 243–274.

Kiecker, C., and Niehrs, C. (2001). A morphogen gradient of Wnt/beta-catenin signalling regulates anteroposterior neural patterning in *Xenopus*. Development *128*, 4189–4201.

Labbé, R.M., Irimia, M., Currie, K.W., Lin, A., Zhu, S.J., Brown, D.D.R., Ross, E.J., Voisin, V., Bader, G.D., Blencowe, B.J., et al. (2012). A comparative transcriptomic analysis reveals conserved features of stem cell pluripotency in planarians and mammals. Stem Cells *30*, 1734–1745.

Lander, R., and Petersen, C.P. (2016). Wnt, Ptk7, and FGFRL expression gradients control trunk positional identity in planarian regeneration. Elife *5*, e02238.

Larsson, M. (2000). High-throughput protein expression of cDNA products as a tool in functional genomics. J. Biotechnol. *80*, 143–157.

Liu, S.-Y., Selck, C., Friedrich, B., Lutz, R., Vila-Farré, M., Dahl, A., Brandl, H., Lakshmanaperumal, N., Henry, I., and Rink, J.C. (2013). Reactivating head regrowth in a regeneration-deficient planarian species. Nature *500*, 81–84.

Lykidis, D., Van Noorden, S., Armstrong, A., Spencer-Dene, B., Li, J., Zhuang, Z., and Stamp, G.W.H. (2007). Novel zinc-based fixative for high quality DNA, RNA and protein analysis. Nucleic Acids Res. *35*, e85.

Mallo, M., Wellik, D.M., and Deschamps, J. (2010). Hox genes and regional patterning of the vertebrate body plan. Dev. Biol. *344*, 7–15.

Meinhardt, H. (1996). Models of biological pattern formation: common mechanism in plant and animal development. Int. J. Dev. Biol. *40*, 123–134.

Meinhardt, H. (2009). Beta-catenin and axis formation in planarians. Bioessays *31*, 5–9.

Molina, M.D., Saló, E., and Cebrià, F. (2007). The BMP pathway is essential for re-specification and maintenance of the dorsoventral axis in regenerating and intact planarians. Dev. Biol. *311*, 79–94.

Morgan, T.H. (1905). "Polarity" considered as a phenomenon of gradation of materials. J. Exp. Zool. *2*, 495–506.

Nacu, E., and Tanaka, E.M. (2011). Limb regeneration: a new development? Annu. Rev. Cell Dev. Biol. *27*, 409–440.

Nogi, T., and Levin, M. (2005). Characterization of innexin gene expression and functional roles of gap-junctional communication in planarian regeneration. Dev. Biol. *287*, 314–335.

Nogi, T., Zhang, D., Chan, J.D., and Marchant, J.S. (2009). A novel biological activity of praziquantel requiring voltage-operated Ca^{2+} channel beta subunits: subversion of flatworm regenerative polarity. PLoS Negl. Trop. Dis. *3*, e464.

Petersen, C.P., and Reddien, P.W. (2008). Smed-betacatenin-1 is required for anteroposterior blastema polarity in planarian regeneration. Science *319*, 327–330.

Petersen, C.P., and Reddien, P.W. (2009). A wound-induced Wnt expression program controls planarian regeneration polarity. Proc. Natl. Acad. Sci. USA *106*, 17061–17066.

Petersen, C.P., and Reddien, P.W. (2011). Polarized notum activation at wounds inhibits Wnt function to promote planarian head regeneration. Science *332*, 852–855.

Reddien, P.W., and Sánchez Alvarado, A. (2004). Fundamentals of planarian regeneration. Annu. Rev. Cell Dev. Biol. *20*, 725–757.

Reddien, P.W., Bermange, A.L., Kicza, A.M., and Sánchez Alvarado, A. (2007). BMP signaling regulates the dorsal planarian midline and is needed for asymmetric regeneration. Development *134*, 4043–4051.

Reuter, H., März, M., Vogg, M.C., Eccles, D., Grífol-Boldú, L., Wehner, D., Owlarn, S., Adell, T., Weidinger, G., and Bartscherer, K. (2015). β-Catenin-dependent control of positional information along the AP body axis in planarians involves a teashirt family member. Cell Rep. *10*, 253–265.

Rink, J.C. (2013). Stem cell systems and regeneration in planaria. Dev. Genes Evol. *223*, 67–84.

Rink, J.C., Gurley, K.A., Elliott, S.A., and Sánchez Alvarado, A. (2009). Planarian Hh signaling regulates regeneration polarity and links Hh pathway evolution to cilia. Science *326*, 1406–1410.

Rouhana, L., Weiss, J.A., Forsthoefel, D.J., Lee, H., King, R.S., Inoue, T., Shibata, N., Agata, K., and Newmark, P.A. (2013). RNA interference by feeding in vitro-synthesized double-stranded RNA to planarians: methodology and dynamics. Dev. Dyn. *242*, 718–730.

Saló, E., and Agata, K. (2012). Planarian regeneration: a classic topic claiming new attention. Int. J. Dev. Biol. *56*, 3–4.

Sánchez Alvarado, A., Newmark, P.A., Robb, S.M., and Juste, R. (2002). The *Schmidtea mediterranea* database as a molecular resource for studying platyhelminthes, stem cells and regeneration. Development *129*, 5659–5665.

Scimone, M.L., Cote, L.E., Rogers, T., and Reddien, P.W. (2016). Two FGFRL-Wnt circuits organize the planarian anteroposterior axis. Elife *5*, e12845.

Sureda-Gómez, M., Pascual-Carreras, E., and Adell, T. (2015). Posterior Wnts have distinct roles in specification and patterning of the planarian posterior region. Int. J. Mol. Sci. *16*, 26543–26554.

Sureda-Gómez, M., Martín-Durán, J.M., and Adell, T. (2016). Localization of planarian βCATENIN-1 reveals multiple roles during anterior-posterior regeneration and organogenesis. Development *143*, 4149–4160.

Turing, A.M. (1952). The chemical basis of morphogenesis. 1953. Philos. Trans. R. Soc. Lond. B Biol. Sci. *237*, 37–72.

Umesono, Y., Tasaki, J., Nishimura, Y., Hrouda, M., Kawaguchi, E., Yazawa, S., Nishimura, O., Hosoda, K., Inoue, T., and Agata, K. (2013). The molecular logic for planarian regeneration along the anterior-posterior axis. Nature *500*, 73–76.

Werner, S., Rink, J.C., Riedel-Kruse, I.H., and Friedrich, B.M. (2014). Shape mode analysis exposes movement patterns in biology: flagella and flatworms as case studies. PLoS One *9*, e113083.

Werner, S., Stückemann, T., Beirán Amigo, M., Rink, J.C., Jülicher, F., and Friedrich, B.M. (2015). Scaling and regeneration of self-organized patterns. Phys. Rev. Lett. *114*, 138101.

Werner, S., Vu, H.T.-K., and Rink, J.C. (2016). Self-organization in development, regeneration and organoids. Curr. Opin. Cell Biol. *44*, 1–8.

Witchley, J.N., Mayer, M., Wagner, D.E., Owen, J.H., and Reddien, P.W. (2013). Muscle cells provide instructions for planarian regeneration. Cell Rep. *4*, 633–641.

Wurtzel, O., Cote, L.E., Poirier, A., Satija, R., Regev, A., and Reddien, P.W. (2015). A generic and cell-type-specific wound response precedes regeneration in planarians. Dev. Cell *35*, 632–645.

STAR★METHODS

KEY RESOURCES TABLE

Reagent or Resource	Source	Identifier
Antibodies		
Mouse monoclonal anti-β-Catenin (clone G78-1)	This paper	N/A
Mouse monoclonal anti-β-Catenin (clone C86-1)	This paper	N/A
Mouse monoclonal anti-PCNA (clone A36-1)	This paper	N/A
Rabbit polyclonal anti-Histone H3	Abcam	Cat#ab1791; RRID: AB_302613
Sheep polyclonal anti-Digoxigenin-AP, Fab fragments	Roche	Cat#11093274910; RRID: AB_514497
IRDye 800CW Goat anti-Mouse IgG	Licor	Cat#925-32210
IRDye 680LT Goat anti-Rabbit IgG	Licor	Cat#925-68021
Chemicals, Peptides, and Recombinant Proteins		
Smed-β-Catenin-1 fragment 1	This paper	N/A
Smed-β-Catenin-1 fragment 8/8	This paper	N/A
TRIzol Reagent	Thermo Fisher Scientific	Cat#15596026
RNAlater	Thermo Fisher Scientific	Cat#AM7021
Critical Commercial Assays		
Novex NuPAGE 4-12% Bis-Tris Protein Gels and MOPS SDS Running Buffer	Thermo Fisher Scientific	Cat#NP0342BOX, Cat#NP0323BOX, Cat#NP0001
nCounter Dx Analysis System and Gene Expression Custom CodeSet	NanoString Technologies	Cat#NCT-SYST-DX-EU, Cat#GXA-P1CS-096
RNeasy Mini Kit	QIAGEN	Cat#74104
SuperScript III First-Strand Synthesis System	Thermo Fisher Scientific	Cat#18080051
RNA 6000 Nano Kit	Agilent	Cat#5067-1511
Deposited Data		
Cloned genes	This paper	GenBank accession numbers KY348643–KY348695
A/P slice RNAseq data; see Table S1	This paper	NCBI SRA Archive, Biosample SAMN06142985
Wnt regulator RNAi Nanostring data; see Table S3	This paper	N/A
Wound-induced expression dynamics of Nanostring genes; see Table S4	This paper	N/A
X1/X2/Xins cell population RNAseq dataset	Labbé et al., 2012	GSE37910
Experimental Models: Organisms/Strains		
Planarian: *Schmidtea mediterranea* asexual CIW4 strain	Sánchez Alvarado et al., 2002	
Recombinant DNA		
pPRT4P vector	Liu et al., 2013	N/A
pAff8c vector	Larsson, 2000	N/A
pGEXK-M12 vector	MPI-CBG Protein Expression and Purification facility	N/A
pETM-11 vector	EMBL Heidelberg	GenBank: CQ878915.1
Sequence-Based Reagents		
Nanostring probes; see Table S2	This paper	N/A
Primers for cloning; see Table S5	This paper	N/A
Primers for RNAi; see Table S5	This paper	N/A
Software and Algorithms		
Matlab	MathWorks	https://www.mathworks.com/products/matlab.html
R	R Foundation	https://www.r-project.org/

(*Continued on next page*)

Continued

Reagent or Resource	Source	Identifier
DEseq R package	EMBL	http://www.bioconductor.org/packages/release/bioc/html/DESeq.html
ImageStudioLite	LI-COR	https://www.licor.com/bio/products/software/image_studio_lite/

CONTACT FOR REAGENT AND RESOURCE SHARING

Further information and requests for resources and reagents should be directed to and will be fulfilled by the Lead Contact (rink@mpi-cbg.de).

EXPERIMENTAL MODEL AND SUBJECT DETAILS

The CIW4 asexual strain of *Schmidtea mediterranea* was used for all experiments.

METHOD DETAILS

Animals, Cloning, and RNAi

Asexual *S. mediterranea* (CIW4 strain) (Sánchez Alvarado et al., 2002) were maintained in 1x Montjuic salts at 20°C, sustained on calf liver and starved for at least 7 days prior to experiments. Dissections were carried out on cold stages set to 4C. For irradiation, animals were exposed to a total dose of 10 000 rads. For cloning, transcript sequences were obtained from PlanMine (Brandl et al., 2016), PCR amplified from cDNA using the primers in Table S5 and inserted into the pPR-T4P vector by ligation-independent cloning. RNAi was carried out either by feeding of dsRNA-expressing HT115 *E. coli* or in vitro synthesized dsRNA mixed with calf liver (1μg dsRNA/μl total food volume) (Gurley et al., 2008; Rouhana et al., 2013). RNAi experimental schedules are provided in Table S6.

Recombinant Proteins and Antibody Production

Two fragments of Smed-β-catenin-1 were produced as recombinant antigen. F1 (aa1-aa239) was cloned into the pAff8c vector (Larsson, 2000) adding N-terminal His- and Albumin binding protein tags, expressed in *E. coli* BL21 and purified over Ni-Agarose under denaturing conditions (6 M Urea) according to standard procedures. Fragment 8/8 (aa834-aa954) was cloned into the pGEXK-M12 vector (MPI-CBG Protein Expression and Purification facility) adding an N-terminal GST-tag, expressed in *E. coli* BL21 and purified over Glutathione matrix according to standard procedures (native purification). The N-terminus of Smed-pcna (aa1-aa125) was cloned into the pETM-11 vector (EMBL Heidelberg) to add an N-terminal His-tag. Monoclonal antibodies were generated by the MPI-CBG antibody facility. Balb/c mice were immunized with recombinant β-catenin-1 fragments (without cleavage of purification tags). Mouse bleeds were screened by Western blotting against wild type and *β-catenin(RNAi)* lysates. Positive mice were sacrificed and immortalized hybrid cells (hybridomas) were obtained by the fusion of splenocytes with the myeloma cell line P3x63Ag8.653 using PEG and AH selection. Hybridoma clones were generated and pre-screened using the Meso Scale Discovery platform (Meso Scale Diagnostics, Rockville, MD) by comparing affinity to the specific β-catenin antigen versus non-specific negative controls, respectively. Positive clones were screened again by Western blotting as above to identify high affinity binders. High affinity binders were subcloned by limiting dilution and retested using the MSD platform. Antibodies were purified using HiTRAP protein G columns (GE Healthcare) followed by acid elution and buffer exchange into PBS pH 7.8. using standard procedures. Two positive clones, Ab-C86-1 (against β-cat fragment 8/8) and Ab-G78-1 (against β-cat fragment F1), were identified as high affinity β-catenin-1 binders and used interchangeably throughout this study. Clone A36-1 recognized Smed-PCNA.

RNA Extraction and RNA Sequencing

Animals were killed in 1% HCl for 1 min and immersed in RNAlater prior to dissection. Total RNA was isolated using the TRIzol (Invitrogen) protocol described in the online supplement of (Eisenhoffer et al., 2008), quality controlled on a Bioanalyzer (Agilent), poly-A selected using Sera-Mag Oligo(dT) beads (Thermo Scientific) and processed for 75 bp-SE Illumina Sequencing (HiSeq 2000) as described previously (Rouhana et al., 2013). dd_Smed_v6 (PCFL) was used as mapping reference. The series of A/P slices in Figure 2A and the regeneration time course experiments (Figure 5D) were both sequenced at 20–30 million single-end 76 bp reads (A/P slices: Single replicates; regeneration time courses: triplicates). The obtained reads were quality checked with FastQC (version v0.10.0). Adaptor and low-quality nucleotides were trimmed with cutadapt (version 0.9.5, trimming option -n 5 -m 20 -q 25). Filtered reads were examined with FastQC again to ensure consistent high quality. The remaining reads were aligned against dd_Smed_v6 using bowtie2 (version 2.1.0). Raw alignment counts per transcript were extracted with bash, and FPKMs were calculated with R.

NanoString Gene Expression Analysis

Approximately 10 animals were killed in RNAlater and cut into six fragments. Corresponding fragments were pooled, homogenized in RLT (Qiagen) buffer supplemented with 40mM DTT, prior to total RNA extraction by phenol-chloroform. The aqueous phase was

precipitated by addition of 1/10 volumes 5 M ammonium acetate, 1/1000 volumes of 10 mg/mL glycogen and 2.5 volumes 100% ethanol and by subsequent incubation at −80°C for at least 1 h. RNA was pelleted by centrifugation at 20.000 rpm at 4°C for 15 min, washed once with 70% ethanol, spun at 20.000 rpm at 4°C for 2 min and air-dried for 4 min. The pellet was dissolved in 25 μL RNAse free water, aliquoted and stored at −80°C. RNA was quality controlled using a Nanodrop spectrophotometer and a Bioanalyzer. 400 pg total RNA were used per Nanostring reaction, following exactly the manufacturer's recommendations. Measured counts were routinely normalized by the H3 transcript (dd_Smed_v5_1920_0_1), but results were comparable even without normalization (due to the equal amounts of input RNA throughout the analysis). Probes were custom designed by Nanostring on basis of ddSmed_v5 transcripts. See Table S2 for probe sequences.

Quantitative Western Blotting

Animals were fixed in zinc fixative for 30 min at RT (0.5% zinc chloride, 0.5% zinc trifluoro acetate, 0.05% calcium acetate in 0.1M Tris–HCl pH 7.0.) (Lykidis et al., 2007), lysed by mechanical pestle homogenization in Urea lysis buffer (6M Urea, 2% SDS, 130 mM DTT, 3.5 u/μl Benzonase, 1x protease inhibitor cocktail consisting of 6μg/ml chymostatin, 0.5μg/ml leupeptin, 10μg/ml antipain-HCl, 2μg/ml aprotinin, 0.7μg/ml pepstatin and 10μg/ml APMSF) incubated for 30 min at RT, clarified by centrifugation and the protein concentration was determined by a Nanodrop spectrophotometer (280 nm). Samples were mixed with 6x Laemmli buffer and frozen at −20°C. Samples were run out in technical quadruplicates on NuPAGE Novex 4–12% Bis-Tris protein gels in 1x MOPS running buffer, transferred onto Nitrocellulose membranes in transfer buffer (1x MOPS with 20% MeOH), blocked in 1x PBS with 0.1% Tween20 and 5% w/v nonfat dry milk and incubated with primary antibody (β-catenin mouse monoclonals at 1 μg/mL; Anti-rabbit Histone H3 antibody (Abcam, ab1791) at 10 ng/mL) in 1x PBS with 0.1% Tween20 and 5% nonfat dry milk. Membranes were washed with washing buffer (1x PBS with 0.1% Tween20) prior to incubation with infrared fluorescent secondary antibodies (anti-Mouse IRDye 800CW, LICOR and anti-Rabbit IRDye 680LT, LICOR) diluted 1:20000 in blocking solution. Membranes were washed with washing buffer, followed by a final wash step in 1x PB without Tween20. Stained membranes were dried and imaged on a LI-COR Odyssey imager. The images were quantified using ImageStudioLite software (see Quantification and Statistical Analysis).

In Situ Hybridization

Whole-mount in situ hybridization was performed as previously described (Liu et al., 2013). Specimens were mounted in mounting media (75% glycerol and 2M urea).

Analysis of β-catenin in FACS-sorted Cells

For FACS analysis of fixed cells, three ~1cm long asexual *S. mediterranea* were de-mucunized in neutralized NAC (0.5% (w/v) N-acetyl cysteine, 20mM HEPES, pH ~7) for 10 min, incubated in maceration solution (13:1:1 ddH_2O: glycerol: acetic acid, modified from (Baguñà, 1976)) for 10 min and an additional 5 min on a rotating wheel. Remaining pieces were dissociated by pipetting up and down, filtered through a 50 μm cell filter (CellTrics, Sysmex) and stained with 60 μg/mL Hoechst 33342 for 30min, RT before FACS. Cells were gated based on Hoechst blue width to exclude doublets and sorted based on Hoechst blue vs. Hoechst red signal. 100,000 cells per population were sorted into 200-250μl maceration solution, centrifuged at 1000 g for 10 min and the supernatant discarded. Tube walls were rinsed twice with 10 μl urea lysis buffer and samples were analyzed by SDS-PAGE and subsequent Western blotting (see above). Primary antibodies were: α-β-catenin-1 (1:4,000), α-PCNA (1:1,000), α-H3 (1:100,000); secondary antibodies conjugated to horseradish peroxidase: α-mouse (1:2,500), α-rabbit (1:2,500). Detection of secondary antibody was performed using two ECL reagents (Luminata Forte (Millipore)) for β-catenin and PCNA; ECL Western Blotting detection reagents (Amersham) for H3).

Imaging

A Nikon AZ100M microscope equipped with a Digital Sight DS-Fi1 camera was used for documenting live images, movies, and NBT/BCIP developed whole-mount in situ specimens.

QUANTIFICATION AND STATISTICAL ANALYSIS

RNAseq Analysis

The regeneration (Table S4) and irradiation time series data (Labbé et al., 2012) was analyzed by the DEseq R-package. Briefly, the raw counts were normalized by the effective library size, obtained via the ''estimateSizeFactors'' function. The relative fold changes with respect to the zero time point and respective adjusted p-values (Benjamini-Hochberg procedure) were obtained with the ''nbinomTest'' function. The moderated log2 fold change was computed based on ''varianceStabilizingTransformation'' together with ''estimateDispersion'' (without pooling replicates, argument ''blind'').

A/P Gene Expression Profile Filtering

The gene expression profiles were filtered by three conditions: (i) at least three successive data points that are non-zero, (ii) the ratio between maximum and minimum value is larger than two, (iii) the standard deviation about the smoothed curve is smaller than 8 times the difference between minimum and maximum value. For the latter, we applied the Savitzky-Golay filter with a first order polynomial in a moving window of 3 data points. The standard deviation about this smoothed curve was computed after removing one outlier data point with the largest deviation from the trend.

A/P Gene Expression Profile Clustering

All clustering was based on the filtered gene expression profiles, normalized to possess a standard deviation of STD=1 about the mean. First, we used a density-based clustering approach to identify groups of genes with highly similar expression profiles (Ester et al., 1996). To this end, we defined a distance between two genes given by the standard deviation of the difference between their respective profiles. For each transcript, the clustering method tested whether there are at least a number N_{min} of other genes in an environment defined by the radius ε. If this was the case, these points were considered clustered. We chose N_{min}=2 and ε=0.14. Note that our method does not require the prior specification of final cluster numbers. Next, we merged the obtained clusters based on similarity, requiring a similarity of ε=0.4. Finally we associated the remaining genes with these clusters if they correlated with the mean cluster profiles with a Pearson coefficient of at least 0.8. The parameters were chosen such that a maximum number of genes was grouped in a minimum number of distinct clusters. Similar clustering results were also obtained for other parameter sets. Genes that could not be clustered are typically either expressed at low levels and thus subject to noise or show a spatially homogeneous expression (not shown).

Quantitative Western Blotting Analysis

All western blot quantifications were conducted using ImageStudioLite software (LICOR). Rectangles were drawn around all β-catenin (protein of interest) and H3 (loading control) bands, and then the background was subtracted from the total signal using the "Median" method (3 pixels border width, top/bottom segment). Each β-catenin signal was then normalized to the corresponding H3 signal, to account for technical variability. Normalised β-catenin signals were then transformed into absolute concentrations (pg β-catenin/μg total protein lysate) using i) the normalized β-catenin signal for the standard sample included in every blot technical replicate, ii) the absolute amount of β-catenin present in this sample (determined by titration against known amounts of recombinant Smed-β-catenin-1), and iii) the total amount of protein lysate loaded for every sample.

DATA AND SOFTWARE AVAILABILITY

All data have been made available online or in the Supplemental Information section of this paper (see Key Resources Table for details). The AP slice gene expression data has also been made available on the PlanMine website (http://planmine.mpi-cbg.de/). All analysis software used in this study is available online (see Key Resources Table for details).